HLH. Histopathological analyses revealed a number of EBER$^+$ cells in the spleen and the liver (Figure 6E) and quantification of EBV DNA in these tissues revealed 1.4×10^1 to 2.4×10^2 copies/μg of EBV DNA. When the tissues were examined by immunostaining and EBER ISH, the EBER$^+$ cells were shown unexpectedly to be mostly CD45RO$^-$ and CD20$^+$ in all five transplantation experiments with four different patients, indicating that the majority of EBV-infected cells in these tissues are of the B-cell lineage (Figure 6E and data not shown). EBER$^+$ large B cells were seen scattered among numerous reactive small T cells, most of which are CD8$^+$, in the tissues of the spleen, liver, lungs and kidneys. A number of macrophages were also seen in these tissues. Fractionation of mononuclear cells obtained from the liver of a mouse transplanted with PBMC of the EBV-HLH patient 10, followed by real-time PCR, detected EBV DNA (1.4×10^1 copies/μg DNA) only in the CD19$^+$ B-cell fraction. In addition, an EBV-infected B lymphoblastoid cell line, but not an EBV-positive T cell line, could be established from this liver. Thus the presence of EBV in B cells were demonstrated by three independent methods in the tissues of EBV-HLH mice. Enzyme-linked immunosorbent assay revealed extremely high levels of human cytokines, including IL-8, IFN-γ, and RANTES, in the sera of both the original patients and the recipient mice (Figure 6B). The levels of IL-8 and IFN-γ were much higher than those observed in the peripheral blood of patients with CAEBV and mice that received their PBMC. Thus, NOG mice transplanted with EBV-HLH-derived PBMC are distinct from those transplanted with CAEBV-derived PBMC in the aggressive time course of the disease, internal hemorrhagic lesions, extremely high levels of IL-8 and IFN-γ in the peripheral blood, and the presence of EBV-infected B cells in lymphoid tissues.

Discussion

The mouse xenograft models of CAEBV and EBV-HLH developed here represent the first recapitulation of EBV-associated T/NK lymphoproliferation in experimental animals. Previously, Hayashi and others inoculated rabbits with Herpesvirus papio and succeeded in the generation of T-cell lymphoproliferative disorder with pathological findings suggestive of EBV-HLH [41]. This model, however, is based on an EBV-related virus and not EBV itself, and therefore may contain features irrelevant to the original human disease. Although the CAEBV and EBV-HLH models described here exhibited some common features, including the abundant presence of EBV-infected T or NK cells in the peripheral blood, there were some critical differences between the two models, probably reflecting the divergence of the pathophysiology of the original diseases. First of all, in the EBV-HLH model mouse, EBV was detected mainly in B cells in the spleen and the liver, while it was found mainly in T cells in the peripheral blood. This makes an obvious contrast with the CAEBV model mouse, where EBV was detected in T or NK cells in both the peripheral blood and lymphoid tissues. We do not have an explanation for the apparent discrepancy in the host cell type of EBV infection between the peripheral blood and lymphoid tissues of the EBV-HLH model. It should be, however, noted that histopathology of EBV-HLH tissues has not been fully investigated and therefore it is still possible that significant number of EBV-infected B cells are present in the lymphoid tissues of EBV-HLH patients. Other differences between the two models include much higher plasma levels of IL-8 and IFN-γ more aggressive and fatal outcome, and internal hemorrhagic lesions in EBV-HLH model mice, probably reflecting the differences in the pathophysiology of the original diseases.

EBV-positive B-cell proliferation was not seen in CAEBV model mice even in long-term observation beyond twelve weeks. This seems puzzling since low but significant amount of EBV DNA was found also in B19$^+$ B-cell fraction in most patients with CAEBV. It should be noted that EBV-infected T or NK cell lines could be established relatively easily from patients with CAEBV by adding recombinant IL-2 in the medium. In contrast, establishment of EBV-infected B LCLs from these patients has been extremely difficult. In fact, we could establish B-LCLs from a few patients with CAEBV only when their PBMC were cultured on feeder cells expressing CD40 ligand. Therefore, we speculate that in the particular context of CAEBV, both in the patient and the model mouse, proliferation of EBV-infected B cells are somehow inhibited by an unknown mechanism.

Analysis on the conditions of engraftment of EBV-infected T/NK cells using these new xenograft models revealed that EBV-infected T and NK cells of the CD8$^+$ T, TCRγδT and CD56$^+$ NK lineages and cell lines derived from them require CD4$^+$ T cells for their engraftment in NOG mice. Only those EBV-infected cells and cell lines of the CD4$^+$ T lineage could engraft in NOG mice on their own. These findings suggest that some factor(s) provided by CD4$^+$ cells are essential for engraftment. Soluble factors produced by CD4$^+$ T cells may be responsible for this function and we are currently examining cytokines, including IL-2, for their ability to support the engraftment of EBV-infected T and NK cells. It is also possible that cell to cell contact involving CD4$^+$ cells is critical for engraftment. This dependence on CD4$^+$ cells represents an interesting consistency with the previous finding that engraftment of EBV-transformed B lymphoblastoid cells in *scid* mice required the presence of CD4$^+$ cells [42,43]. It has been speculated that T cells activated by an EBV-induced superantigen may be involved in the engraftment of EBV-infected B lymphoblastoid cells in *scid* mice [44]. Although a similar superantigen-mediated mechanism might also be assumed in T- and NK-cell lymphoproliferation in NOG mice, the data of TCR repertoire analyses (Figure 1C and data not shown) show no indication for clonal expansion of Vβ13 T cells that are known to be specifically activated by the EBV-induced superantigen HERV-K18. It seems therefore unlikely that this superantigen is involved in the CD4$^+$ T cell-dependent engraftment of EBV-infected T and NK cells. We expect CD4$^+$ T cells and/or molecules produced by them may be an excellent target in novel therapeutic strategies for the treatment of CAEBV and EBV-HLH. In fact, administration of the OKT-4 antibody that depletes CD4$^+$ cells in vivo efficiently prevented the engraftment of EBV-infected T cells. As a next step, we plan to test the effect of post-engraftment administration of OKT-4.

The dependence of EBV-infected T and NK cells on CD4$^+$ T cells for their engraftment in NOG mice suggests the possibility that these cells are not capable of autonomous proliferation. Consistent with this notion, EBV-infected T and NK cell lines, including that of the CD4$^+$ lineage, are dependent on IL-2 for their in vitro growth and do not engraft in either nude mice or *scid* mice when transplanted either s.c. or i.v (Shimizu, N., unpublished results). Clinically, CAEBV is a disease of chronic time course and patients carrying monoclonal EBV-infected T or NK cell population may live for many years without progression of the disease [15]. Overt malignant T or NK lymphoma usually develops only after a long course of the disease. Taking all these findings in consideration, we suppose that EBV-infected cells are not truly malignant at least in the early phase of the disease, even when they appear monoclonal. Because infection of EBV in T or NK cells is not unique to CAEBV and has been recognized also in infectious mononucleosis [45,46], the critical deficiency in

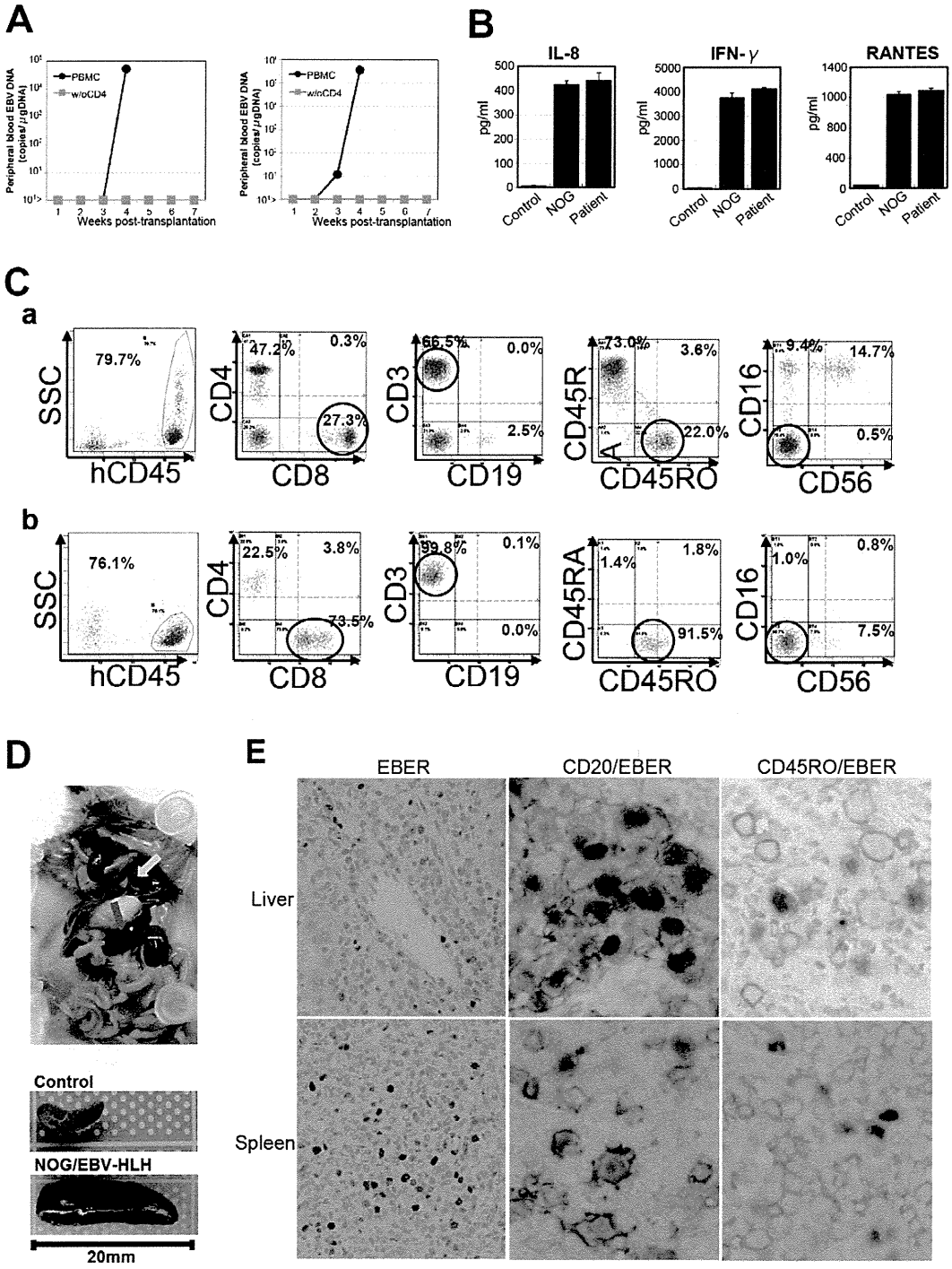

Figure 6. Engraftment of EBV-infected T and B cells in NOG mice transplanted with PBMC of patients with EBV-HLH. A. Peripheral blood EBV DNA load. Following transplantation with PBMC or PBMC devoid of $CD4^+$ cells of the patient 11, EBV DNA was measured weekly by real-time PCR. Results of two mice prepared in an experiment are shown. B. Cytokine levels in the peripheral blood of the patient 12 and a mouse that received his PBMC. The levels of IL-8, IFN-γ, and RANTES were measured by ELISA in triplicates and the means and the standard errors are shown. A plasma sample of healthy person was used as a control. C. Immunophenotypic analyses on the peripheral blood lymphocytes of the EBV-HLH patient 10 (a) and a mouse that received his PBMC (b). Lymphocytes were gated by the pattern of the side scatter and the expression of human CD45, and analyzed for the expression of the indicated markers. The circles indicate the fractions that contained EBV DNA. D. Photograph of a mouse showing splenomegaly (red arrow) and hemorrhagic lesions (yellow arrow). Spleens excised from this mouse and a control mouse are shown at the bottom. E. Photomicrographs of the tissues of mice transplanted with EBV-HLH-derived PBMC. Liver and spleen tissues of a mouse transplanted with PBMC of the patient 11 were examined by EBER-ISH (left), double staining with an anti-human CD20 monoclonal antibody and EBER-ISH (middle), and double staining with an anti-human CD45RO monoclonal antibody and EBER-ISH (right). Original magnification ×600.
doi:10.1371/journal.ppat.1002326.g006

CAEBV may be its inability to immunologically remove EBV-infected T and NK cells. In this context, it should be emphasized that EBV-infected T or NK cells usually exhibit the latency II pattern of EBV gene expression and do not express EBNA3s, that possess immuno-dominant epitopes recognized by EBV-specific T cells [47]. EBV-infected T and NK cells are thus not likely to be removed by cytotoxic T cells as efficiently as EBV-infected B cells that express EBNA3s. The reported lack of cytotoxic T cells specific to LMP2A [17], one of the few immuno-dominant EBV proteins expressed in the virus-infected T and NK cells, may therefore seriously affect the host's capacity to control their proliferation. A genetic defect in the perforin gene was recently identified in a patient with clinical and pathological features resembling CAEBV, suggesting that defects in genes involved in immune responses can result in clinical conditions similar to CAEBV [48].

Engraftment of EBV-infected T and NK cells in NOG mice was in most cases accompanied by co-engraftment of un-infected cell populations. These un-infected cells might have been maintained and induced to proliferate by certain factors produced by EBV-infected T or NK cells. Abundant cytokines produced by these cells may be responsible for this activity. It is also possible that the proliferation of these un-infected cells represents immune responses. Experiments are underway to test whether these un-infected T cells contain EBV-specific cells. These un-infected T cells might also be reacting to host murine tissues. Intravenous injection of PBMC obtained from normal humans to immunodeficient mice including NOG mice has been shown to induce acute or chronic graft versus host disease (GVHD) [49,50]. However, because much less PBMC were injected to mice in the present study as compared to those previous studies, it is not likely that major GVHD was induced in NOG mice transplanted with PBMC of patients with CAEBV or EBV-HLH.

CAEBV has been treated by a variety of regimens, including antiviral, cytocidal, and immunomodulating agents with more or less unsatisfactory results. Although hematopoietic stem cell transplantation, especially that with reduced intensity conditioning can give complete remission in a substantial number of patients [51,52], it is still desirable to develop safer and more effective treatment, possibly with pharmaceutical agents. The xenograft model of CAEBV generated in this study may be an excellent animal model to test novel experimental therapies for the disease. In fact, the OKT-4 antibody that depletes $CD4^+$ T cells in vivo gave a promising result implying its effectiveness as a therapeutic to CAEBV.

Materials and Methods

Ethics statement

Protocols of the experiments with materials obtained from patients with CAEBV and EBV-HLH and from control persons have been reviewed and approved by the Institutional Review Boards of the National Center for Child Health and Development and of the National Institute of Infectious diseases (NIID). Blood samples of the patients and control persons were collected after obtaining written informed consent. Protocols of the experiments with NOG mice are in accordance with the Guidelines for Animal Experimentation of the Japanese Association for Laboratory Animal Science and were approved by the Institutional Animal Care and Use Committee of NIID.

Patients with CAEBV and EBV-HLH

Characteristics of the nine patients with CAEBV and the four patients with EBV-HLH examined in this study are summarized in Table 1. Diagnosis of CAEBV and EBV-HLH was made on the basis of the published guidelines [19,53] and confirmed by identification of EBV-infected T or NK cells in their peripheral blood by flow cytometry and real-time PCR.

NOD/Shi-*scid*/IL2Rγ^{null} (NOG) mice

Mice of the NOD/Shi-*scid*/IL-2Rγ^{null} (NOG) strain [22] were obtained from the Central Institute for Experimental Animals (Kawasaki, Japan) and maintained under specific pathogen free (SPF) conditions in the animal facility of NIID, as described [22].

Transplantation of PBMC or their subfractions to NOG mice

PBMC were isolated by centrifugation on Lymphosepar I (Immuno-Biological Laboratories (IBL)) and injected intravenously to the tail vein of NOG mice at the age of 6–8 weeks. Depending on the recovery of PBMC, $1–4\times10^6$ cells were injected to 2 to 4 mice in a typical experiment with a blood sample. For transplantation with individual cellular fractions containing EBV DNA, $CD4^+$ T cells, $CD8^+$ T cells, and $CD56^+$ NK cells were separated with the IMag Cell Separation Systems (BD Pharmingen) following the protocol supplied by the manufacturer. To isolate γδT cells, $CD19^+$, $CD4^+$, $CD8^+$, $CD56^+$, and $CD14^+$ cells were serially removed from PBMC by the IMag Cell Separation Systems. From the remaining $CD19^-CD4^-CD8^-CD56^-CD14^-$ population, $CD3^+$ cells were positively selected by the same kit and defined as the γδT cell fraction. To transplant PBMC lacking individual immunophenotypic subsets, $CD19^+$, $CD4^+$, $CD8^+$, $CD56^+$ or $CD14^+$ cells were removed from PBMC by the IMag Cell Separation Systems and the remaining cells were injected to mice. To prepare PBMC lacking γδT cells, $CD19^+$, $CD4^+$, $CD8^+$, $CD56^+$, and $CD14^+$ cells isolated from PBMC in the process of obtaining γδT cell fraction (see above) were pooled and mixed with the $CD19^-CD4^-CD8^-CD56^-CD14^-$ cells that did not react with anti-CD3 antibody. For complementation experiments, an EBV-containing cell fraction and the $CD4^+$ cell fraction were isolated from a sample of PBMC as described above and the mixture of these two fractions were injected to NOG mice. The approximate numbers of injected cells are shown in Table 2.

Analysis of immunophenotypes and TCR repertoire expression by flow cytometry

PBMC isolated from the patients and the recipient NOG mice as described above were incubated for 30 min on ice with a mixture of appropriate combinations of fluorescently labeled monoclonal antibodies. After washing, five-color flow-cytometric analysis was carried out with the Cytomics FC500 analyzer (Beckman Coulter). The following directly labeled antibodies were used: phycoerythrin (PE)-conjugated antibodies to CD3, CD8, and TCRα/β, fluorescein isothiocyanate (FITC)-conjugated antibodies to CD3, CD4, CD8, CD19, TCRVγ9, TCRVδ2, and TCRγ/δ, and Phycoerythrin Texas Red (ECD)-conjugated antibody to CD45RO from Beckman Coulter; PE-conjugated antibodies to CD16, CD40, and CD40L, and FITC-conjugated antibody to CD56 from BD Pharmingen. TCR Vβ repertoire analysis was performed with the Multi-analysis TCR Vβ antibodies Kit (Beckman Coulter) according to the procedure recommended by the manufacturer.

Treatment of mice with the OKT-4 antibody

NOG mice were injected intravenously with 5×10^6 PBMC isolated from the CAEBV patient 3 (CD8 type) or 8 (NK type) and were subsequently injected intravenously with 100 μg of the OKT-4 antibody on the same day of transplantation. Additional

administration of the antibody was carried out by the same dose and route for the following three consecutive days. Peripheral blood EBV DNA load was then monitored every week. Mice were finally sacrificed four weeks post-transplantation and applied for pathological and virological analyses.

Quantification of EBV DNA by real time PCR and analysis of EBV gene expression by RT-PCR

Quantification of EBV DNA was carried out by real-time quantitative PCR assay based on the TaqMan system (Applied Biosystems), as described [54]. Analysis of EBV gene expression by RT-PCR was carried out as previously described with the following primers [55]. EBNA1: sense, gatgagcgtttgggagagctgattctgca; antisense, tcctcgtccatggttatcac. EBNA2: sense, agaggaggtggtaagcggttc; antisense, tgacgggtttccaagactatcc. LMP1: sense, ctctccttctcctcctcttg; antisense, caggagggtgatcatcagta. LMP2A: sense, atgactcatctcaacacata; antisense, catgttaggcaaattgcaaa. LMP2B: sense, cagtgtaatctgcacaaaga; antisense, catgttaggcaaattgcaaa. EBER1: sense, agcacctacgctgccctaga; antisense, aaaacatgcggaccaccagc. Cp-EBNA1: sense,cactacaagacctacgcctctccattcatc; anti sense, ttcggtctcccctaggccctg. Wp/Cp-EBNA1: sense, tcagagcgccaggagtccacacaaat; antisense, ttcggtctcccctaggccctg. Qp-EBNA1: sense, aggcgcgggatagcgtgcgctaccgga; antisense, tcctcgtccatggttatcac. RT-PCR primers for β-actin were purchased from Takara (Osaka, Japan).

Histopathology, EBER ISH, and immunohistochemistry

Tissue samples were fixed in 10% buffered formalin, embedded in paraffin, and stained with hematoxylin and eosin. For phenotypic analysis of engrafted lymphocytes, immunostaining for CD3, CD8 (Nichirei), CD45RO, and CD20 (DAKO) was performed on paraffin sections. EBV was detected by in situ hybridization (ISH) with EBV small RNA (EBER) probe. Immunohistochemistry and ISH were performed on an automated stainer (BENCHMARK XT, Ventana Medical Systems) according to the manufacturer's recommendations. To determine the cell lineage of EBV infected cells, paraffin sections were applied to double staining with EBER ISH and immunohistochemistry. Immediately following EBER ISH, immunostaining for CD45RO or CD20 was performed. Photomicrographs was acquired with a OLYMPUS BX51 microscope equipped with 40x/0.75 and 20x/0.50 Uplan Fl objective lens, a Pixera Penguin 600CL digital camera (Pixera), and Viewfinder 3.01 (Pixera) for white balance, contrast, and brightness correction.

Quantification of cytokines

The levels of human IL-8, IFN-γ, and RANTES in plasma samples were measured with the Enzyme-linked immunosorbent assay (ELISA) kit provided by R&D Systems following instructions provided by the manufacturer.

Accession numbers

The Swiss-Prot accession numbers for the proteins described in this article are as follows: P13501 for RANTES; P10145 for IL-8; P01579 for IFN-γ; P03211 for EBNA1; P12978 for EBNA2; P12977 for EBNA3; P03230 for LMP1; and Q66562 for LMP2. The DDBJ accession number for EBER is AJ315772.

Supporting Information

Figure S1 Changes in the body weight of NOG mice transplanted with PBMC derived from patients with CAEBV or EBV-HLH. Body weight of the five CAEBV mice shown in Figure 1A (transplanted with PBMC from the patient 1, 3, 5, and 9, and with the $CD4^+$ fraction from the patient 1, respectively) and two EBV-HLH mice shown in Figure 6A (both transplanted with PBMC from the patient 11) were recorded weekly.
(TIF)

Figure S2 Histopathological analysis of a control NOG mouse. A. a NOG mouse without xenograft. A 20-week old female NOG mouse was sacrificed and examined as a reference. No human cells are identified in these tissues. Upper panels: liver tissue was stained with hematoxylin-eosin (HE), antibodies specific to human CD3 or CD20, or by ISH with an EBER probe; the rightmost panel is a double staining with EBER and human CD45RO. Bottom panels: EBER ISH in the spleen, kidney, and small intestine. B. a NOG mouse transplanted with PBMC of a healthy EBV carrier. A six-week old female NOG mouse was transplanted with 5×10^6 PBMC isolated from a normal EBV-seropositive person and sacrificed at eight weeks post-transplantation for histological analysis. Liver and Spleen tissues were stained with HE, antibodies specific to human CD3 or CD20, or by ISH with an EBER probe. No EBER-positive cells were identified in these tissues.Original magnification is ×200 for both A and B.
(TIF)

Table S1 EBV DNA load in lymphocyte subsets of a patient with CAEBV and a corresponding mouse derived from her PBMC.
(DOC)

Table S2 EBV DNA load in lymphocyte subsets of a patient with EBV-HLH and a corresponding mouse derived from his PBMC.
(DOC)

Acknowledgments

We thank Kumiko Tanaka, Ken Watanabe, and Miki Katayama for technical assistance.

Author Contributions

Conceived and designed the experiments: KI MY NS NY SF. Performed the experiments: KI MY AN FK SI HN. Analyzed the data: KI MY AN SF. Contributed reagents/materials/analysis tools: AA TM SO MI OM JK. Wrote the paper: KI SF.

References

1. Rickinson AB, Kieff ED (2007) Epstein-Barr virus. In: Knipe DM, Howley PM, eds. Fields Virology 5. ed. Philadelphia: Lippincott Williams and Wilkins. pp 2655–2700.
2. Kieff ED, Rickinson AB (2007) Epstein-Barr virus and its replication. In: Knipe DM, Howley PM, eds. Fields Virology. Philadelphia: Lippincott Williams and Wilkins. pp 2603–2654.
3. Fujiwara S, Ono Y (1995) Isolation of Epstein-Barr virus-infected clones of the human T-cell line MT-2: use of recombinant viruses with a positive selection marker. J Virol 69: 3900–3903.
4. Watry D, Hedrick JA, Siervo S, Rhodes G, Lamberti JJ, et al. (1991) Infection of human thymocytes by Epstein-Barr virus. J Exp Med 173: 971–980.
5. Kikuta H, Sakiyama Y, Matsumoto S, Oh-Ishi T, Nakano T, et al. (1993) Fatal Epstein-Barr virus-associated hemophagocytic syndrome. Blood 82: 3259–3264.
6. Kawaguchi H, Miyashita T, Herbst H, Niedobitek G, Asada M, et al. (1993) Epstein-Barr virus-infected T lymphocytes in Epstein-Barr virus-associated hemophagocytic syndrome. J Clin Invest 92: 1444–1450.
7. Kawa-Ha K, Ishihara S, Ninomiya T, Yumura-Yagi K, Hara J, et al. (1989) CD3-negative lymphoproliferative disease of granular lymphocytes containing Epstein-Barr viral DNA. J Clin Invest 84: 51–55.
8. Jones JF, Shurin S, Abramowsky C, Tubbs RR, Sciotto CG, et al. (1988) T-cell lymphomas containing Epstein-Barr viral DNA in patients with chronic Epstein-Barr virus infections. N Engl J Med 318: 733–741.

9. Kikuta H, Taguchi Y, Tomizawa K, Kojima K, Kawamura N, et al. (1988) Epstein-Barr virus genome-positive T lymphocytes in a boy with chronic active EBV infection associated with Kawasaki-like disease. Nature 333: 455–457.
10. Ishihara S, Tawa A, Yumura-Yagi K, Murata M, Hara J, et al. (1989) Clonal T-cell lymphoproliferation containing Epstein-Barr (EB) virus DNA in a patient with chronic active EB virus infection. Jpn J Cancer Res 80: 99–101.
11. Jaffe ES (2009) The 2008 WHO classification of lymphomas: implications for clinical practice and translational research. Hematology Am Soc Hematol Educ Program 2009: 523–531.
12. Okano M (2002) Overview and problematic standpoints of severe chronic active Epstein-Barr virus infection syndrome. Crit Rev Oncol Hematol 44: 273–282.
13. Straus SE (1992) Acute progressive Epstein-Barr virus infections. Annu Rev Med 43: 437–449.
14. Kimura H (2006) Pathogenesis of chronic active Epstein-Barr virus infection: is this an infectious disease, lymphoproliferative disorder, or immunodeficiency? Rev Med Virol 16: 251–261.
15. Kimura H, Morishima T, Kanegane H, Ohga S, Hoshino Y, et al. (2003) Prognostic factors for chronic active Epstein-Barr virus infection. J Infect Dis 187: 527–533.
16. Tsuge I, Morishima T, Kimura H, Kuzushima K, Matsuoka H (2001) Impaired cytotoxic T lymphocyte response to Epstein-Barr virus-infected NK cells in patients with severe chronic active EBV infection. J Med Virol 64: 141–148.
17. Sugaya N, Kimura H, Hara S, Hoshino Y, Kojima S, et al. (2004) Quantitative analysis of Epstein-Barr virus (EBV)-specific CD8+ T cells in patients with chronic active EBV infection. J Infect Dis 190: 985–988.
18. Aoukaty A, Lee IF, Wu J, Tan R (2003) Chronic active Epstein-Barr virus infection associated with low expression of leukocyte-associated immunoglobulin-like receptor-1 (LAIR-1) on natural killer cells. J Clin Immunol 23: 141–145.
19. Henter JI, Horne A, Arico M, Egeler RM, Filipovich AH, et al. (2007) HLH-2004: Diagnostic and therapeutic guidelines for hemophagocytic lymphohistiocytosis. Pediatr Blood Cancer 48: 124–131.
20. Lay JD, Tsao CJ, Chen JY, Kadin ME, Su IJ (1997) Upregulation of tumor necrosis factor-alpha gene by Epstein-Barr virus and activation of macrophages in Epstein-Barr virus-infected T cells in the pathogenesis of hemophagocytic syndrome. J Clin Invest 100: 1969–1979.
21. Imashuku S, Hibi S, Ohara T, Iwai A, Sako M, et al. (1999) Effective control of Epstein-Barr virus-related hemophagocytic lymphohistiocytosis with immunochemotherapy. Histiocyte Society. Blood 93: 1869–1874.
22. Ito M, Hiramatsu H, Kobayashi K, Suzue K, Kawahata M, et al. (2002) NOD/SCID/gamma(c)(null) mouse: an excellent recipient mouse model for engraftment of human cells. Blood 100: 3175–3182.
23. Shultz LD, Lyons BL, Burzenski LM, Gott B, Chen X, et al. (2005) Human lymphoid and myeloid cell development in NOD/LtSz-scid IL2R gamma null mice engrafted with mobilized human hemopoietic stem cells. J Immunol 174: 6477–6489.
24. Strowig T, Gurer C, Ploss A, Liu YF, Arrey F, et al. (2009) Priming of protective T cell responses against virus-induced tumors in mice with human immune system components. J Exp Med 206: 1423–1434.
25. Watanabe S, Terashima K, Ohta S, Horibata S, Yajima M, et al. (2007) Hematopoietic stem cell-engrafted NOD/SCID/IL2Rgamma null mice develop human lymphoid systems and induce long-lasting HIV-1 infection with specific humoral immune responses. Blood 109: 212–218.
26. Yajima M, Imadome K, Nakagawa A, Watanabe S, Terashima K, et al. (2008) A new humanized mouse model of Epstein-Barr virus infection that reproduces persistent infection, lymphoproliferative disorder, and cell-mediated and humoral immune responses. J Infect Dis 198: 673–682.
27. Traggiai E, Chicha L, Mazzucchelli L, Bronz L, Piffaretti JC, et al. (2004) Development of a human adaptive immune system in cord blood cell-transplanted mice. Science 304: 104–107.
28. Melkus MW, Estes JD, Padgett-Thomas A, Gatlin J, Denton PW, et al. (2006) Humanized mice mount specific adaptive and innate immune responses to EBV and TSST-1. Nat Med 12: 1316–1322.
29. Baenziger S, Tussiwand R, Schlaepfer E, Mazzucchelli L, Heikenwalder M, et al. (2006) Disseminated and sustained HIV infection in CD34+ cord blood cell-transplanted Rag2-/-gamma c-/- mice. Proc Natl Acad Sci U S A 103: 15951–15956.
30. Zhang L, Kovalev GI, Su L (2007) HIV-1 infection and pathogenesis in a novel humanized mouse model. Blood 109: 2978–2981.
31. Dewan MZ, Watanabe M, Ahmed S, Terashima K, Horiuchi S, et al. (2005) Hodgkin's lymphoma cells are efficiently engrafted and tumor marker CD30 is expressed with constitutive nuclear factor-kappaB activity in unconditioned NOD/SCID/gammac(null) mice. Cancer Sci 96: 466–473.
32. Ishikawa F, Yoshida S, Saito Y, Hijikata A, Kitamura H, et al. (2007) Chemotherapy-resistant human AML stem cells home to and engraft within the bone-marrow endosteal region. Nat Biotechnol 25: 1315–1321.
33. Durig J, Ebeling P, Grabellus F, Sorg UR, Mollmann M, et al. (2007) A novel nonobese diabetic/severe combined immunodeficient xenograft model for chronic lymphocytic leukemia reflects important clinical characteristics of the disease. Cancer Res 67: 8653–8661.
34. Nakagawa A, Ito M, Saga S (2002) Fatal cytotoxic T-cell proliferation in chronic active Epstein-Barr virus infection in childhood. Am J Clin Pathol 117: 283–290.
35. Nagata H, Konno A, Kimura N, Zhang Y, Kimura M, et al. (2001) Characterization of novel natural killer (NK)-cell and gammadelta T-cell lines established from primary lesions of nasal T/NK-cell lymphomas associated with the Epstein-Barr virus. Blood 97: 708–713.
36. Imai S, Sugiura M, Oikawa O, Koizumi S, Hirao M, et al. (1996) Epstein-Barr virus (EBV)-carrying and -expressing T-cell lines established from severe chronic active EBV infection. Blood 87: 1446–1457.
37. Yoshioka M, Ishiguro N, Ishiko H, Ma X, Kikuta H, et al. (2001) Heterogeneous, restricted patterns of Epstein-Barr virus (EBV) latent gene expression in patients with chronic active EBV infection. J Gen Virol 82: 2385–2392.
38. Kimura H, Hoshino Y, Hara S, Sugaya N, Kawada J, et al. (2005) Differences between T cell-type and natural killer cell-type chronic active Epstein-Barr virus infection. J Infect Dis 191: 531–539.
39. Xu J, Ahmad A, Jones JF, Dolcetti R, Vaccher E, et al. (2000) Elevated serum transforming growth factor beta1 levels in Epstein-Barr virus-associated diseases and their correlation with virus-specific immunoglobulin A (IgA) and IgM. J Virol 74: 2443–2446.
40. Ohga S, Nomura A, Takada H, Ihara K, Kawakami K, et al. (2001) Epstein-Barr virus (EBV) load and cytokine gene expression in activated T cells of chronic active EBV infection. J Infect Dis 183: 1–7.
41. Hayashi K, Ohara N, Teramoto N, Onoda S, Chen HL, et al. (2001) An animal model for human EBV-associated hemophagocytic syndrome: herpesvirus papio frequently induces fatal lymphoproliferative disorders with hemophagocytic syndrome in rabbits. Am J Pathol 158: 1533–1542.
42. Veronese ML, Veronesi A, D'Andrea E, Del Mistro A, Indraccolo S, et al. (1992) Lymphoproliferative disease in human peripheral blood mononuclear cell-injected SCID mice. I. T lymphocyte requirement for B cell tumor generation. J Exp Med 176: 1763–1767.
43. Johannessen I, Asghar M, Crawford DH (2000) Essential role for T cells in human B-cell lymphoproliferative disease development in severe combined immunodeficient mice. Br J Haematol 109: 600–610.
44. Sutkowski N, Palkama T, Ciurli C, Sekaly RP, Thorley-Lawson DA, et al. (1996) An Epstein-Barr virus-associated superantigen. J Exp Med 184: 971–980.
45. Anagnostopoulos I, Hummel M, Kreschel C, Stein H (1995) Morphology, immunophenotype, and distribution of latently and/or productively Epstein-Barr virus-infected cells in acute infectious mononucleosis: implications for the interindividual infection route of Epstein-Barr virus. Blood 85: 744–750.
46. Hudnall SD, Ge Y, Wei L, Yang NP, Wang HQ, et al. (2005) Distribution and phenotype of Epstein-Barr virus-infected cells in human pharyngeal tonsils. Mod Pathol 18: 519–527.
47. Hislop AD, Taylor GS, Sauce D, Rickinson AB (2007) Cellular responses to viral infection in humans: lessons from Epstein-Barr virus. Annu Rev Immunol 25: 587–617.
48. Katano H, Ali MA, Patera AC, Catalfamo M, Jaffe ES, et al. (2004) Chronic active Epstein-Barr virus infection associated with mutations in perforin that impair its maturation. Blood 103: 1244–1252.
49. van Rijn RS, Simonetti ER, Hagenbeek A, Hogenes MC, de Weger RA, et al. (2003) A new xenograft model for graft-versus-host disease by intravenous transfer of human peripheral blood mononuclear cells in RAG2-/- gammac-/- double-mutant mice. Blood 102: 2522–2531.
50. Ito R, Katano I, Kawai K, Hirata H, Ogura T, et al. (2009) Highly sensitive model for xenogenic GVHD using severe immunodeficient NOG mice. Transplantation 87: 1654–1658.
51. Kawa K, Sawada A, Sato M, Okamura T, Sakata N, et al. (2011) Excellent outcome of allogeneic hematopoietic SCT with reduced-intensity conditioning for the treatment of chronic active EBV infection. Bone Marrow Transplant 46: 77–83.
52. Sato E, Ohga S, Kuroda H, Yoshiba F, Nishimura M, et al. (2008) Allogeneic hematopoietic stem cell transplantation for Epstein-Barr virus-associated T/natural killer-cell lymphoproliferative disease in Japan. Am J Hematol 83: 721–727.
53. Okano M, Kawa K, Kimura H, Yachie A, Wakiguchi H, et al. (2005) Proposed guidelines for diagnosing chronic active Epstein-Barr virus infection. Am J Hematol 80: 64–69.
54. Kimura H, Morita M, Yabuta Y, Kuzushima K, Kato K, et al. (1999) Quantitative analysis of Epstein-Barr virus load by using a real-time PCR assay. J Clin Microbiol 37: 132–136.
55. Nakamura H, Iwakiri D, Ono Y, Fujiwara S (1998) Epstein-Barr-virus-infected human T-cell line with a unique pattern of viral-gene expression. Int J Cancer 76: 587–594.

Epstein-Barr Virus Induces Erosive Arthritis in Humanized Mice

Yoshikazu Kuwana[1☯], Masami Takei[1*☯], Misako Yajima[2], Ken-Ichi Imadome[3], Hirotake Inomata[1], Masaaki Shiozaki[1], Natsumi Ikumi[1], Takamasa Nozaki[1], Hidetaka Shiraiwa[1], Noboru Kitamura[1], Jin Takeuchi[1], Shigemasa Sawada[1], Naoki Yamamoto[2], Norio Shimizu[4], Mamoru Ito[5], Shigeyoshi Fujiwara[3*]

1 Division of Hematology and Rheumatology, Department of Medicine, Nihon University School of Medicine, Tokyo, Japan, **2** Department of Microbiology, Yong Loo Lin School of Medicine, National University of Singapore, Singapore, **3** Department of Infectious Diseases, National Research Institute for Child Health and Development, Tokyo, Japan, **4** Department of Virology, Division of Medical Science, Medical Research Institute, Tokyo Medical and Dental University, Tokyo, Japan, **5** Central Institute for Experimental Animals, Kawasaki, Japan

Abstract

Epstein-Barr virus (EBV) has been implicated in the pathogenesis of rheumatoid arthritis (RA) on the basis of indirect evidence, such as its presence in affected joint tissues, antigenic cross reactions between EBV and human proteins, and elevated humoral and cellular anti-EBV immune responses in patients. Here we report development of erosive arthritis closely resembling RA in humanized mice inoculated with EBV. Human immune system components were reconstituted in mice of the NOD/Shi-*scid*/IL-2Rγ^{null} (NOG) strain by transplantation with $CD34^+$ hematopoietic stem cells isolated from cord blood. These humanized mice were then inoculated with EBV and examined pathologically for the signs of arthritis. Erosive arthritis accompanied by synovial membrane proliferation, pannus formation, and bone marrow edema developed in fifteen of twenty-three NOG mice transplanted with human HSC and inoculated with EBV, but not in the nine NOG mice that were transplanted with HSC but not inoculated with EBV. This is the first report of an animal model of EBV-induced arthritis and strongly suggest a causative role of the virus in RA.

Citation: Kuwana Y, Takei M, Yajima M, Imadome K-I, Inomata H, et al. (2011) Epstein-Barr Virus Induces Erosive Arthritis in Humanized Mice. PLoS ONE 6(10): e26630. doi:10.1371/journal.pone.0026630

Editor: Matthias G. von Herrath, La Jolla Institute of Allergy and Immunology, United States of America

Received August 26, 2011; **Accepted** September 29, 2011; **Published** October 19, 2011

Funding: This study was supported by grants from the Ministry of Health, Labour and Welfare of Japan (H22-Nanchi-080 and H22-AIDS-002:http://www.mhlw.go.jp/), the Grant of National Center for Child Health and Development (22A-9:http://www.ncchd.go.jp/), and Strategic Research Base Development; Program for Private Universities subsidized by MEXT (S0801033 2010: http://www.mext.go.jp/a_menu/koutou/shinkou/07021403/002/002/1218299.htm). The funders had no role in study design, data collection and analysis, decision to publish, or preparation of the manuscript.

Competing Interests: The authors have declared that no competing interests exist.

* E-mail: takei.masami@ nihon-u.ac.jp (MT); shige@nch.go.jp (SF)

☯ These authors contributed equally to this work.

Introduction

A number of observations including those by the authors have suggested the involvement of Epstein-Barr virus (EBV) in the pathogenesis of rheumatoid arthritis (RA)[1,2,3,4,5,6,7]. For example, circulating EBV load is higher in RA patients than in healthy controls [8] and activated CD8-positive cells specific to EBV are commonly seen in RA patients[9]. Further, studies have reported that a large number of T cells specific to EBV-encoded proteins are present in the affected joints of RA patients[10], that interference of suppressor T cells specific to EBV plays a role in RA[11], and that RA patients have abnormally large numbers of EBV-infected B cells in the blood[12]. We have reported on the decreased expression of the gene coding for the signaling lymphocytic activation molecule-associated protein (SAP) (also known as the Src homology 2 domain-containing protein 1A (SH2D1A)) that is supposed to have critical roles in the elimination of EBV-infected B cells by cytotoxic T cells and NK cells [13]. This reduced expression of SAP might lead to the failure of the immune system to eliminate EBV-infected B cells in RA patients [14]. These studies, however, provided only indirect evidence for the involvement of EBV in RA and there have been no published reports on EBV-induced arthritis in experimental animals.

Although model animals for EBV infection are required to examine a causal relationship between EBV and RA, there has been no appropriate animal models suitable for this purpose. EBV can infect only limited primate species and does not infect normal mice. Recently, we developed a humanized mouse model of EBV infection, based on the NOD/Shi-*scid*/IL-2Rγ^{null} (NOG) mouse strain[15], that can reproduce key aspects of human EBV infection, such as lymphoproliferative disorder, asymptomatic persistent infection, and humoral and T cell–mediated immune responses[15]. In this model, where human immune components were reconstituted by transplantation with cord blood-derived $CD34^+$ stem cells, inoculation with high-dose EBV ($\sim 1\times10^3$ 50% transformation dose [TD_{50}]) resulted in the development of lymphoproliferative disorder, whereas inoculation with low-dose virus ($<1\times10^1$ TD50) tended to cause apparently asymptomatic persistent infection [15]. Immunological analyses of these mice demonstrated the presence of EBV-specific $CD8^+$ T cells that inhibit transformation of autologous B lymphocytes by the virus [16]. In the present study, we characterized histopathology of joint tissues obtained from EBV-infected humanized NOG mice and

demonstrated erosive arthritis with many features resembling those of RA.

Materials and Methods

Ethics Statement and Preparation of humanized mice

NOG mice were obtained from the Central Institute for Experimental Animals (Kawasaki, Japan), and protocols for experiments with NOG mice were approved by the Institutional Animal Care and Use Committee of the National Institute of Infectious Diseases (NIID; Tokyo, Japan) (certification number 206061, 14th. April 2006). Cord blood was obtained from the Tokyo Cord Blood Bank (Tokyo, Japan) after acquiring informed consent from the parents of the donors. Protocols for experiments with human materials were approved by the Institutional Review Boards of the National Research Institute for Child Health and Development (Tokyo, Japan) (certification number 139, 22th. March 2005), the NIID (certification number 1, 17th. October 1997), and the Tokyo Cord Blood Bank (certification number 06-17-02, 18th. August 2006). Isolation of human $CD34^+$ HSCs from cord blood using the MACS Direct CD34 Progenitor Cell Isolation Kit (Miltenyi Biotec, Bergisch Gladbach, Germany), their intravenous injection (1×10^4 to 1.2×10^5 cells/mouse) into 6- to 10-week-old female NOG mice, and characterization of reconstitution of human hematoimmune system components in these mice were performed as described elsewhere[17]. NOG mice were not irradiated prior to transplantation with $CD34^+$ HSCs, because they lived significantly longer after humanization and satisfactory development of human immune system components were observed without irradiation [18]. NOG mice in which human hematoimmune system components were reconstituted are referred to here as humanized NOG (hNOG) mice.

Analysis on the reconstitution of human lymphoid system components in hNOG mice

Peripheral blood mononuclear cells were isolated weekly from NOG mice following transplantion with human $CD34^+$ stem cells and examined for the reactivity with the following antibodies by flow cytometry: FITC-conjugated anti–human CD45 (J.33), CD3 (UCHT1), CD4 (13B8.2), CD19 (J4.119), and CD45RO (UCHL1) (all from Beckman Coulter, Brea, CA); PE-conjugated anti–human CD4 (13B8.2), CD8 (B9.11), CD19 (J4.119), CD45RA (ALB11) (all from Beckman Coulter), and CXCR4 (44717; R&D Systems, Minneapolis, MN); anti–mouse CD45 (YW62.3; Beckman Coulter); ECD-conjugated anti–human CD45 (J.33; Beckman Coulter); and PC5-conjugated anti–human CD8 (T8) and CD14 (Rm052) (all from Beckman Coulter). Flow cytometric analysis was conducted by 2- or 4-color staining using the EpicsXL flow cytometer (Beckman Coulter).

Experimental EBV infection and quantification of viral DNA

Supernatant fluid of Akata cell culture was prepared as described previously[15] and used as EBV inoculum. EBV dose in 50% transformation dose (TD_{50}) was determined by a standard method as described previously[15]. EBV was inoculated intravenously through the tail vein. Peripheral blood EBV DNA load was quantified by real-time polymerase chain reaction (PCR) based on the TaqMan system (Applied Biosystems), as described elsewhere[19]. As a control, nine hNOG mice were left uninfected; among them four mice were inoculated with supernatant fluid of EBV-negative Akata cell culture.

Histopathology, in situ hybridization (ISH), and immunohistochemistry

hNOG mice were sacrificed 1 to 12 months after inoculation with EBV and their major joints including knees and ankles were removed and fixed in 10% formalin solution. These specimens were embedded in paraffin and stained with hematoxylin-eosin (HE) for histological examinations. For phenotypic analysis of proliferating lymphocytes, immunostaining with the antibodies specific to human CD3 (DAKO, A0452), CD4 (Leica, NCL-CD4-1F6), CD8 (Leica, NCL-CD8-4B11), CD20 (DAKO, M0755) and CD68 (DAKO, M0876) was performed on paraffin sections. EBV was detected by in-situ hybridization (ISH) with EBV-encoded small RNA (EBER) probes (DAKO, Y5200).

Statistical Analysis

Fisher's exact test was used for categorical data. Analyses were performed using JMP 7.0.2 for Windows (SAS Institute Inc., Cary, NC). All tests were two-tailed, with differences reported as significant when p values were less than 0.01.

Results

Twenty-three hNOG mice, prepared with $CD34^+$ cells isolated from ten different cord blood samples and inoculated with EBV were examined histopathologically for the presence of erosive arthritis. The number of transplanted $CD34^+$ cells ($0.1–1.2\times10^5$ cells), days from transplantation with $CD34^+$ cells to inoculation with EBV (106–197 days), dose of EBV inoculated ($10^0–10^3$ TD_{50}), days from EBV inoculation to autopsy (26–320 days) for each mouse are described in Table S1. As a control, nine hNOG mice prepared with $CD34^+$ cells isolated from three different cord blood samples and not inoculated with EBV were examined similarly (Table S1). Among them, four mice were mock inoculated with culture supernatant of EBV-negative Akata cells. HE staining of major joints including knees and ankles revealed synovial proliferation and infiltration of inflammatory cells in the synovium in 15 of the 23 EBV-infected hNOG mice (65%), whereas none of the nine control hNOG mice showed these signs of arthritis ($P = 0.001$ by the two-tailed Fisher's exact test) (Fig. 1A and Table 1). Development of arthritis was not dependent on viral dose, because hNOG mice developed arthritis following EBV inoculation at each dose (10^0, 10^1, 10^2, 10^3 TD_{50}) (Table S1). The earliest time point when arthritis was observed was 26 days post-infection and it was seen as late as 320 days post-infection. In a fraction of examined mice, granulation tissue overgrew the bearing surface of the joint and was associated with the breakdown of the articular surface. Furthermore, multinuclear giant cells similar to osteoclasts were seen in the granulation tissue that invaded the bone on the joint edge (Figure 1A). This histology is remarkably similar to the pannus formation seen in erosive arthritis characteristic to RA. In the bone marrow adjacent to inflamed joints, infiltration of activated mononuclear cells generated a histology reminiscent of bone marrow edema characteristic to RA (Fig. 1A).

Immunostaining with monoclonal antibodies revealed a large number of CD3-positive T cells among the proliferating cells in the synovial tissue (Fig. 1B). Both $CD4^+$ and $CD8^+$ cells were identified. There were also a few $CD20^+$ B cells and $CD68^+$ macrophages. When the bone marrow adjacent to inflamed joint tissue was examined by immunostaining, CD3-positive cells and CD4-positive cells were detected, while almost no cells exhibited positive CD20 staining (Figure 1B). It should be noted that because NOG mice lack T, B, and NK lymphocytes completely and human-specific antibodies were used here, all lymphocytes detected in hNOG mouse tissues are considered to be of human origin. EBER ISH revealed only few EBV-infected

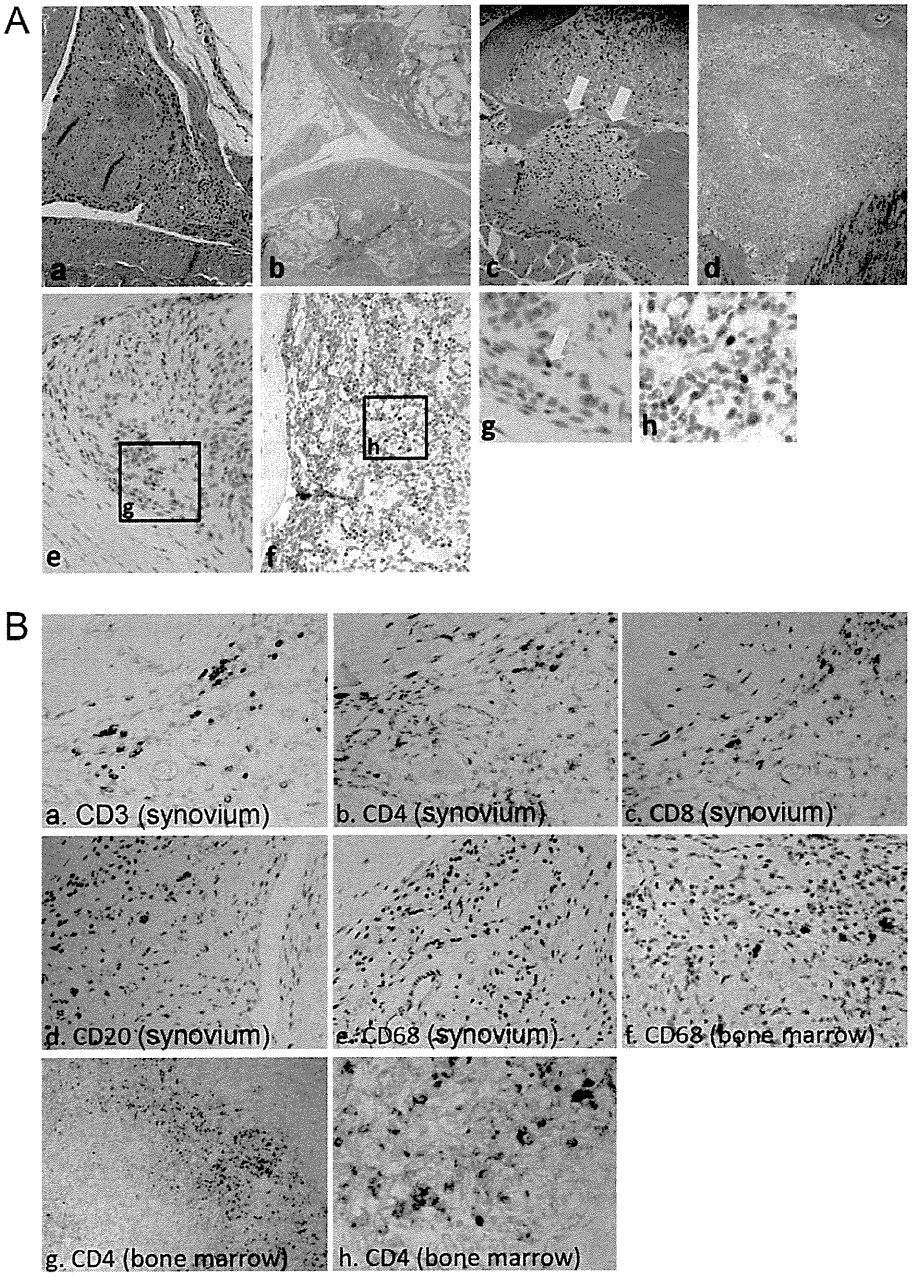

Figure 1. Histopathology of joint and adjacent bone marrow tissues in hNOG mice infected with EBV. A. HE staining and EBER ISH. HE staining of a knee joint in the EBV-infected mouse N70-13 (Table S1), showing synovial proliferation (a): a knee joint in the control mouse N69-1 not infected with EBV (b): a knee joint in the EBV-infected mouse N87-6 (Table S1), showing a pannus-like lesion containing multinuclear giant cells (yellow arrows) (c): and bone marrow near the knee joint of N70-13, showing edema (d). EBER ISH in the synovium of a knee joint in the EBV-infected mouse N79-1 (Table S1), showing few EBV-infected cells (e), and in the bone marrow adjacent to the affected knee joint of the same mouse, demonstrating a number of EBV-infected cells (f). g and h represent further magnification of a portion of e and f, respectively. The yellow arrow indicates an $EBER^+$ cell. Original magnification, ×200 (a, c, d, e, f), ×100 (b). B. Immunostaining. Joint (a–e) and adjacent bone marrow tissues (f–h) from the N70-13 mouse were examined for the expression of CD3 (a), CD4 (b, g, h), CD8 (c), CD20 (d), and CD68 (e, f). Original magnification; x200 (a–b), x400 (c–f), x100 (g), x400 (h).
doi:10.1371/journal.pone.0026630.g001

cells in the synovial membrane of affected joints (Fig. 1A), whereas numerous EBV-infected cells were detected in the bone marrow near the affected joints (Fig. 1A).

Discussion

Erosive arthritis was observed in 15 among the 23 hNOG mice infected with EBV but not in nine control mice that were reconstituted with human immune system components but not inoculated with EBV. The incidence of erosive arthritis is significantly elevated among EBV-infected mice compared with control uninfected mice ($P = 0.001$ by the two-tailed Fisher's exact test). This erosive arthritis is accompanied by pannus formation, synovial membrane proliferation, inflammatory cell infiltration to the synovium, and bone marrow edema, rendering it closely similar to the tissue of RA. In addition, numerous EBER-positive

Table 1. Development of arthritis in EBV-infected hNOG mice.

Arthritis	EBV-infected	Un-infected
(+)	15 *	0
(−)	8	9

*p = 0.001, by two-tailed Fisher's exact test.
doi:10.1371/journal.pone.0026630.t001

cells were seen in the edematous bone marrow adjacent to the affected joint. Thus, these results provide the first evidence that EBV can induce erosive arthritis resembling RA in experimental animals. We examined whether anti-cyclic citrullinated peptide (CCP) antibodies and rheumatoid factor (RF), two major markers of RA, were present in the blood of hNOG, but neither was detected.

Few EBER-positive cells were detected in the synovium of affected mouse joints and therefore it is unlikely that EBV-infected cells elicited strong virus-specific immune responses in the synovium and these immune responses triggered aberrant effects damaging the surrounding tissue. However, as numerous $CD4^+$ T cells, as well as $EBER^+$ cells, were found in the edematous bone marrow adjacent to the affected joint, it is conceivable that migration of inflammatory cells from bone marrow to synovium via ostioles, as Ochi an others suggested, had a role in the initiation of erosive arthritis [20]. It is also possible that inflammatory cytokines produced in bone marrow diffused through the nutrient canal or the nutrient foramen to the synovium and induce the proliferation of synoviocytes and the activation of osteoclasts in the adjacent joint. Significant levels (150–200 pg/ml) of IFN-γ were detected in the plasma of EBV-infected humanized mice. Antigenic cross reaction between EBV proteins and host mouse tissues might have been also involved in the pathogenesis of erosive arthritis in the mice. It should be noted, however, that after rigorous examination we have not detected anti-EBV antibodies in EBV-infected hNOG mice, except for anti-$p18^{BFRF3}$ (the18-kDa protein encoded by the third rightward open reading frame in the BamHI F fragment) IgM antibody shown in four out of thirty examined mice[15]. We did not detect antibodies to either EBNA1 that cross-reacts with a 62 kDa protein found in the synovium affected by RA [5] or gp110 that cross-reacts with HLA-DR [6,21]. Antigenic mimicry involving humoral immune responses may thus be unlikely to have a major role in the pathogenesis of erosive arthritis in hNOG mice. In contrast, we observed abundant T-cell response to EBV infection in hNOG mice[15,16] and it is conceivable that these strong T-cell response has some role in the generation of erosive arthritis.

The present mouse model of erosive arthritis may be an excellent system to investigate the pathogenesis of RA. In this model, it is feasible to remove particular cellular or molecular factors implicated in the pathogenesis of RA by administration of specific antibodies or specific functional antagonists[16]. Analysis on the effects of these antibodies or antagonists will clarify the role of individual cellular and molecular components of the immune system and hence give new insights to the pathogenesis of RA. In a similar approach, this model can also be used to search for molecular and/or cellular targets of novel therapeutics for RA.

Supporting Information

Table S1 hNOG mice examined for the development of arthritis.
(DOC)

Acknowledgments

We thank Ms. Eiko Ishizuka and Mr. Hiroyuki Masuda for their excellent technical assistance.

Author Contributions

Conceived and designed the experiments: MT SF. Performed the experiments: YK MY K-II TN NK MS NS NY NI. Analyzed the data: MS HS NS NY SS MT YK MY SF JT. Wrote the paper: MT YK HI. Mainly wrote the manuscript: MT YK. Corrected the grammar and spelling of the manuscript: HI. Supervised the project: MT. Produced and provided NOG mice: MI. Performed the computational and statistical data analyses: YK HI.

References

1. Alspaugh MA, Jensen FC, Rabin H, Tan EM (1978) Lymphocytes transformed by Epstein-Barr virus. Induction of nuclear antigen reactive with antibody in rheumatoid arthritis. J Exp Med 147: 1018–1027.
2. Billings PB, Hoch SO, White PJ, Carson DA, Vaughan JH (1983) Antibodies to the Epstein-Barr virus nuclear antigen and to rheumatoid arthritis nuclear antigen identify the same polypeptide. Proc Natl Acad Sci U S A 80: 7104–7108.
3. Rhodes G, Carson DA, Valbracht J, Houghten R, Vaughan JH (1985) Human immune responses to synthetic peptides from the Epstein-Barr nuclear antigen. J Immunol 134: 211–216.
4. Rumpold H, Rhodes GH, Bloch PL, Carson DA, Vaughan JH (1987) The glycine-alanine repeating region is the major epitope of the Epstein-Barr nuclear antigen-1 (EBNA-1). J Immunol 138: 593–599.
5. Fox R, Sportsman R, Rhodes G, Luka J, Pearson G, et al. (1986) Rheumatoid arthritis synovial membrane contains a 62,000-molecular-weight protein that shares an antigenic epitope with the Epstein-Barr virus-encoded associated nuclear antigen. J Clin Invest 77: 1539–1547.
6. Roudier J, Rhodes G, Petersen J, Vaughan JH, Carson DA (1988) The Epstein-Barr virus glycoprotein gp110, a molecular link between HLA DR4, HLA DR1, and rheumatoid arthritis. Scand J Immunol 27: 367–371.
7. Takei M, Mitamura K, Fujiwara S, Horie T, Ryu J, et al. (1997) Detection of Epstein-Barr virus-encoded small RNA 1 and latent membrane protein 1 in synovial lining cells from rheumatoid arthritis patients. Int Immunol 9: 739–743.
8. Balandraud N, Meynard JB, Auger I, Sovran H, Mugnier B, et al. (2003) Epstein-Barr virus load in the peripheral blood of patients with rheumatoid arthritis: accurate quantification using real-time polymerase chain reaction. Arthritis Rheum 48: 1223–1228.
9. Lunemann JD, Frey O, Eidner T, Baier M, Roberts S, et al. (2008) Increased frequency of EBV-specific effector memory CD8+ T cells correlates with higher viral load in rheumatoid arthritis. J Immunol 181: 991–1000.
10. Scotet E, David-Ameline J, Peyrat MA, Moreau-Aubry A, Pinczon D, et al. (1996) T cell response to Epstein-Barr virus transactivators in chronic rheumatoid arthritis. J Exp Med 184: 1791–1800.
11. Tosato G, Steinberg AD, Blaese RM (1981) Defective EBV-specific suppressor T-cell function in rheumatoid arthritis. N Engl J Med 305: 1238–1243.
12. Tosato G, Steinberg AD, Yarchoan R, Heilman CA, Pike SE, et al. (1984) Abnormally elevated frequency of Epstein-Barr virus-infected B cells in the blood of patients with rheumatoid arthritis. J Clin Invest 73: 1789–1795.
13. Filipovich AH, Zhang K, Snow AL, Marsh RA (2010) X-linked lymphoproliferative syndromes: brothers or distant cousins? Blood 116: 3398–3408.
14. Takei M, Ishiwata T, Mitamura K, Fujiwara S, Sasaki K, et al. (2001) Decreased expression of signaling lymphocytic-activation molecule-associated protein (SAP) transcripts in T cells from patients with rheumatoid arthritis. Int Immunol 13: 559–565.
15. Yajima M, Imadome K, Nakagawa A, Watanabe S, Terashima K, et al. (2008) A new humanized mouse model of Epstein-Barr virus infection that reproduces persistent infection, lymphoproliferative disorder, and cell-mediated and humoral immune responses. J Infect Dis 198: 673–682.
16. Yajima M, Imadome K, Nakagawa A, Watanabe S, Terashima K, et al. (2009) T cell-mediated control of Epstein-Barr virus infection in humanized mice. J Infect Dis 200: 1611–1615.
17. Watanabe S, Terashima K, Ohta S, Horibata S, Yajima M, et al. (2007) Hematopoietic stem cell-engrafted NOD/SCID/IL2Rgamma null mice develop

human lymphoid systems and induce long-lasting HIV-1 infection with specific humoral immune responses. Blood 109: 212–218.
18. Watanabe S, Ohta S, Yajima M, Terashima K, Ito M, et al. (2007) Humanized NOD/SCID/IL2Rgamma(null) mice transplanted with hematopoietic stem cells under nonmyeloablative conditions show prolonged life spans and allow detailed analysis of human immunodeficiency virus type 1 pathogenesis. J Virol 81: 13259–13264.
19. Kimura H, Morita M, Yabuta Y, Kuzushima K, Kato K, et al. (1999) Quantitative analysis of Epstein-Barr virus load by using a real-time PCR assay. J Clin Microbiol 37: 132–136.
20. Ochi T, Hakomori S, Adachi M, Owaki H, Okamura M, et al. (1988) The presence of a myeloid cell population showing strong reactivity with monoclonal antibody directed to difucosyl type 2 chain in epiphyseal bone marrow adjacent to joints affected with rheumatoid arthritis (RA) and its absence in the corresponding normal and non-RA bone marrow. J Rheumatol 15: 1609–1615.
21. Roudier J, Petersen J, Rhodes GH, Luka J, Carson DA (1989) Susceptibility to rheumatoid arthritis maps to a T-cell epitope shared by the HLA-Dw4 DR beta-1 chain and the Epstein-Barr virus glycoprotein gp110. Proc Natl Acad Sci U S A 86: 5104–5108.

Epstein-Barr Virus BART9 miRNA Modulates LMP1 Levels and Affects Growth Rate of Nasal NK T Cell Lymphomas

Rajesh Ramakrishnan[1], Hart Donahue[1], David Garcia[1], Jie Tan[1], Norio Shimizu[2], Andrew P. Rice[1], Paul D. Ling[1]*

1 Department of Molecular Virology & Microbiology, Baylor College of Medicine, Houston, Texas, United States of America, **2** Department of Virology, Division of Virology & Immunology, Medical Research Institute, Tokyo Medical and Dental University, Tokyo, Japan

Abstract

Nasal NK/T cell lymphomas (NKTCL) are a subset of aggressive Epstein-Barr virus (EBV)-associated non-Hodgkin's lymphomas. The role of EBV in pathogenesis of NKTCL is not clear. Intriguingly, EBV encodes more than 40 microRNAs (miRNA) that are differentially expressed and largely conserved in lymphocryptoviruses. While miRNAs play a critical role in the pathogenesis of cancer, especially lymphomas, the expression and function of EBV transcribed miRNAs in NKTCL are not known. To examine the role of EBV miRNAs in NKTCL, we used microarray profiling and qRT-PCR to identify and validate expression of viral miRNAs in SNK6 and SNT16 cells, which are two independently derived NKTCL cell lines that maintain the type II EBV latency program. All EBV BART miRNAs except BHRF-derived miRNAs were expressed and some of these miRNAs are expressed at higher levels than in nasopharyngeal carcinomas. Modulating the expression of BART9 with antisense RNAs consistently reduced SNK6 and SNT16 proliferation, while antisense RNAs to BARTs-7 and -17-5p affected proliferation only in SNK6 cells. Furthermore, the EBV LMP-1 oncoprotein and transcript levels were repressed when an inhibitor of BART9 miRNA was transfected into SNK6 cells, and overexpression of BART9 miRNA increased LMP-1 protein and mRNA expression. Our data indicate that BART9 is involved in NKTCL proliferation, and one of its mechanisms of action appears to be regulating LMP-1 levels. Our findings may have direct application for improving NKTCL diagnosis and for developing possible novel treatment approaches for this tumor, for which current chemotherapeutic drugs have limited effectiveness.

Citation: Ramakrishnan R, Donahue H, Garcia D, Tan J, Shimizu N, et al. (2011) Epstein-Barr Virus BART9 miRNA Modulates LMP1 Levels and Affects Growth Rate of Nasal NK T Cell Lymphomas. PLoS ONE 6(11): e27271. doi:10.1371/journal.pone.0027271

Editor: Maria G. Masucci, Karolinska Institutet, Sweden

Received September 2, 2011; **Accepted** October 13, 2011; **Published** November 10, 2011

Funding: This project was supported in part by the Baylor–UT Houston Center for AIDS Research Core Support Grant number AI036211 from the National Institute of Allergy and Infectious Diseases to APR and PDL. RR was supported by NIH grant T32AI7456. No additional external funding received for this study. The funders had no role in study design, data collection and analysis, decision to publish, or preparation of the manuscript.

Competing Interests: The authors have declared that no competing interests exist.

* E-mail: pling@bcm.edu

Introduction

EBV is a member of the herpes virus family and is a pre-eminent human oncogenic virus with a causal relationship to several malignancies, including endemic Burkitt's lymphoma (eBL), nasopharyngeal carcinoma (NPC), a proportion of gastric carcinomas (GC), NKT-cell lymphomas (NKTCL), Hodgkin disease (HD), post-transplant lymphoma-like disease (PTLD), and leiomyosarcomas [1,2]. Within the context of AIDS, EBV is associated with a proportion of non-Hodgkin lymphomas, almost all HD, and leiomyosarcomas. The EBV genome contains over 170,000 bp encoding more than 80 genes. EBV gene expression during latency and tumorgenesis consists of distinct combinations of six nuclear proteins (EBNAs), three membrane proteins (LMPs) and multiple noncoding RNAs, including over 40 miRNAs [3,4,5,6,7]. While the EBV latent proteins have been investigated intensively for some time, the contribution of EBV-encoded miRNAs or altered cellular miRNA expression in EBV-induced cancers has not been fully explored.

The EBV miRNAs were the first viral encoded miRNAs discovered [6]. MiRNAs are ~22 nt transcripts that form imperfect duplexes with target mRNAs and thereby inhibit their expression. MiRNAs typically target the 3′ UTR of mRNAs and the average magnitude of repression of the encoded protein is ~30% [8]. EBV miRNAs are primarily derived from a group of alternatively spiced RNAs transcribed from the BamH1A region of the genome (BamA rightward transcripts or BARTs) [3,4,5,6]. The BARTs encode a large number of miRNAs and with the exception of mir-BART2; the majority are derived from two clusters. A cluster of 3 miRNAs has also been identified which are derived from the BHRF1 gene. The sum total of at least 40 EBV-encoded miRNAs dramatically increases the complexity of potentially biologically active molecules encoded by EBV during latent infection [9]. Like many of the miRNAs discovered to date, the functions of the EBV-encoded miRNAs remain poorly understood. It has been hypothesized that herpesvirus miRNAs, including those encoded by EBV, Cytomegalovirus (CMV), and Kaposi's sarcoma- associated Herpesvirus (KHSV), may facilitate the viral life cycle by blocking innate or adaptive immune responses or by interfering with the appropriate regulation of apoptosis, cell growth, or DNA replication in infected cells [9]. Herpesvirus miRNAs might also target mRNAs for viral genes that regulate the productive lytic cycle, thus having a role in maintaining latency or modulating productive lytic infection. EBV-encoded miRNAs can target both viral and cellular genes. EBV mir-BART2 targets the EBV DNA polymerase mRNA for degradation [10], which inhibits lytic replication and miRNAs from BART cluster 1 may target the viral LMP-1 protein [11]. In

addition, mir-BART5 targets the pro-apoptotic factor PUMA and mir-BHRF1-3 targets the chemokine/T-cell attractant CXCL11 [12,13]. Dysregulation of cellular miRNAs following B cell infection has also been described [11,14,15,16,17]. The cellular miRNAs 146a and 155 regulate lymphocyte signaling and gene expression pathways in this context.

Three general patterns of viral gene expression have been identified in EBV-associated cancers [1,2]. Latency I is characterized by expression of EBNA-1, while latency II is characterized by expression of EBNA-1 along with LMP1 and 2. Latency III is characterized by expression of all EBNAs and LMPs and is typically associated with B cells infected with EBV in vitro or in lymphomas in the immunosuppressed. EBV miRNAs are expressed in all EBV infected tumor cells, although they are differentially expressed in some tumors [3,4,5,6,7,18,19,20,21]. The context in which miRNA functions are investigated may be particularly important since the ubiquitous and powerful activities of all the latent proteins expressed in latency III could mask some of the activities contributed by miRNAs. Recently, several cell lines have been isolated from EBV-associated NKT cell lymphomas, which appear to select for latency II in both primary tumor tissues as well as the cell lines [22,23]. Thus, NKTCL cell lines may be a powerful model system to investigate the functions of EBV gene products within the context of latency II and may lead to insights into miRNA functions in EBV-associated HD, GC, and NPC, for which few practical cell culture systems are available.

Nasal NK/T cell lymphomas (NKTCL) are a heterogeneous group of tumors, so named because some tumors have an NK phenotype ($CD3^-$, $CD56^+$) and some have a T cell phenotype (usually $CD4^+/CD3^+$, but sometimes $CD8^+$ $CD3^+$ and sometimes $CD3^+$ 4^-, 8^- gamma delta) [24,25]. NKTCL is a distinct clinical entity characterized by necrotic lesions in the nasal cavity, nasopharynx, and palate. These are generally aggressive tumors with poor prognosis [24,25]. A universal feature of these tumors is the consistent and strong association with EBV, although the precise role of the virus in this disease remains poorly understood. Analysis of primary tumor tissue has shown a latency II pattern of EBV gene expression [22,23]. At least 7 cell lines of both NK and T cell-like phenotypes have been derived from primary tumors. These include NK-like ($CD3^-$, $CD56^+$) SNK1, -6, -10 and T-cell-like ($CD3^+$, $CD56^+$, $TCR\gamma/\delta^+$) SNT 8, -13, 15, -16 cell lines [22,23]. The cell lines, like the primary tumor tissues from which they were derived, retain latency II EBV expression patterns and the EBV genome is clonal. EBV expresses more than 40 miRNAs, but which ones are expressed in NKTCL remains unknown. We hypothesized that specific viral and cellular miRNAs are likely to play a role in the genesis and maintenance of NKTCL. To address this, we utilized microarrays and quantitative PCR to identify EBV miRNAs that are expressed in established NKTCL cell lines. Transfection of antisense oligonucleotides to some of the abundantly expressed EBV miRNAs revealed that at least one of them, BART9, contributes significantly to NKTCL proliferation. The results provide new information about the expression pattern of EBV encoded miRNAs in NKTCLs and identified a novel function for the EBV-encoded BART9 miRNA.

Results

NKTCL stably maintain the EBV Type II latency program

In tumors, EBV displays latency programs characterized by specific patterns of viral gene expression. In Burkitt's lymphoma, Type I latency is seen while Type II latency is observed in nasopharyngeal carcinoma, gastric carcinoma, and Hodgkin's disease. Type III latency is often restricted to B lymphomas in immunodeficient patients [26]. Although previous studies have found that NKTCLs have a type II latency phenotype, it is common for some EBV positive cell lines to drift towards type III latency in culture. To confirm the latency phenotype under our culture conditions, we tested five NKTCL cell lines for latent and lytic gene expression. We found that the two SNK (SNK6 and SNK10) and three SNT (SNT8, SNT15 and SNT16) cell lines expressed EBNA1 and LMP1 (Figure 1A). These cell lines did not express the other EBNA proteins, EBNA-LP, EBNA3C and EBNA2 (Figure 1B). We also found that there was no expression of

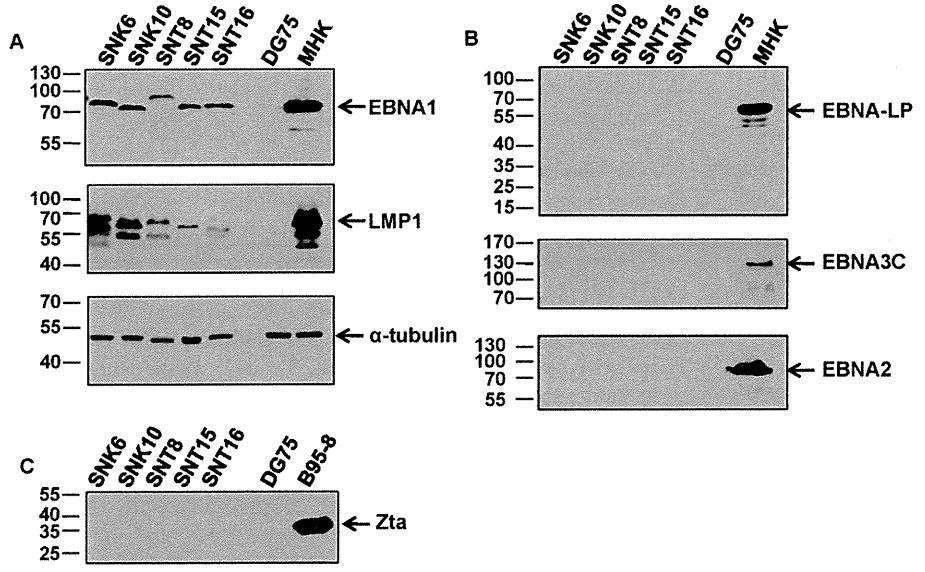

Figure 1. Characterization of NK T cell lymphoma cell lines by immunoblot analysis. Cell lysates were prepared from two NK-like (SNK6, SNK10) and three T cell-like (SNT8, SNT15 and SNT16) NKTCLs. Immunoblots were performed to analyze the expression of the indicated EBV latent and lytic proteins. EBV negative DG75 cells were used as a negative control and EBV positive MHK cells, which maintain Latency III gene expression and express all of the latent proteins, were used as a positive control.
doi:10.1371/journal.pone.0027271.g001

Zta lytic protein (Figure 1C). These data indicate that the NKTCL cell lines stably exhibit a Type II latency program.

miRNA microarray profiling of NKTCL

Nasal NK/T cell lymphomas (NKTCLs) have been demonstrated to be consistently associated with Epstein-Barr virus (EBV) as all cases are EBV positive [27,28,29]. EBV encodes at least 40 microRNAs (miRNA) [3] and there is increasing evidence for the role that miRNAs play in malignant transformation of cells [30]. Therefore, to investigate the role of EBV miRNAs in NKTCL oncogenesis, we first carried out miRNA microarray profiling. We isolated total RNA from two representative NKTCL cell lines, SNK6 and SNT16. Both SNK6 and SNT16 express cellular and EBV proteins that are consistent with prototypical NK and T-cell like NKTCLs respectively. These cell lines were also chosen for microarray profiling and further analysis because of their robust growth and viability in cell culture relative to other known SNK or SNT cell lines. A miRHumanVirus microarray chip was used to examine the expression levels of 1100 mature miRNAs that included human (875) and viral (225) miRNAs. The probes also included 44 EBV miRNAs in the microarray chip.

We used the criteria and statistical parameters described in the Methods to analyze the EBV miRNA expression patterns in the two NKTCL cell lines. Using a median expression value cut-off of 500, we identified 19–21 EBV miRNAs that were present at relatively high levels in SNK6 and SNT16 cell lines (Fig. 2A). To verify the reliability of the microarray data, we selected seven EBV miRNAs whose expression in the microarray ranged from high to low and carried out Taqman PCR on total RNA extracted from SNK6 and SNT16 cells. To more easily compare the relative expression levels of these miRNAs to previous studies, miRNA levels are shown normalized to either 10 pg total RNA or as copy numbers per cell. As shown in Figure 2B and C, the relative expression level of EBV miRNAs BART17-5p, BART7, BART1-3p, BART9, and BART10 was at least one log higher than EBV miRNA BART2-3p in both SNK6 and SNT16 cells. The levels of the miRNAs were also higher in SNT16 cells than SNK6 cells. This is in agreement with the microarray data which also showed a higher expression level of the selected miRNAs in SNT16 cells compared to SNK6 cells (Fig. 2B). Notably, BHRF1 derived miRNAs were nearly undetectable (Fig. 2A–C). These data indicate that the microarray profiling data are generally reliable and this analysis has therefore determined the set of EBV miRNAs which are expressed in the SNK6 and SNT16 cell lines.

Reducing EBV miRNA levels affect SNK6 and SNT16 growth rate

miRNAs regulate many genes including, those involved in cell growth [31]. We first investigated the consequences of blocking EBV miRNA function on the growth rate of SNK6 and SNT16 NKT-cell lines. Based on the miRNA microarray profile (Fig. 2), we chose six EBV miRNAs that were expressed at high levels in both cell lines. The six EBV miRNAs were individually inhibited by transfection LNA-modified antisense oligonucleotides. Samples were collected every 24 hours for three days and cell numbers and viability analyzed. The anti-EBV-miR-BART9, anti-EBV-miR-BART7 and anti-miR- BART17-5p showed a statistically significant reduction in SNK6 cell growth (~19%, ~20% and ~29%, respectively) (Fig. 3A). EBV-miR-BART1-5p and EBV-miR-BART16 antisense oligonucleotides did not have statistically significant effects on SNK6 growth rate. Also there was no significant effect on the viability of the SNK6 cells upon inhibition of any of the EBV miRNAs shown in Figure 3A (Fig. 3B). In SNT16 cells, only anti-EBV-miR-BART9 showed a statistically significant decrease (~34%) in cell growth. Anti-EBV-miR-BART16, anti-EBV-miR-BART17-5p, anti-EBV-miR-BART7, anti-EBV-miR1-5p affected cell growth by ~25%, ~3%, ~10% and ~7%, respectively, but these differences were not statistically significant in a paired t-test (Fig. 3C). We noted that there was a decrease of ~20% in viability of SNT16 cells when the levels of EBV miRNAs were reduced (data not shown). Anti-EBV-miR-BART1-3p showed an increase in SNK6 and SNT16 cell growth, but this difference was not statistically significant (Fig. 3A and C). A scrambled control miRNA had no detectable effect on proliferation or viability on either cell line (Fig. 3). This data suggests that the expression levels of some EBV miRNAs may play a role in cell proliferation.

Inhibiting EBV miR-BART9 reduces LMP1 protein and mRNA expression in SNK6 cells

Because reducing BART9 levels affected growth rate in SNK6 and SNT16 cells (Fig. 3), we focused further experiments on the BART9 miRNA. EBV-encoded LMP1 triggers multiple cellular signaling pathways that influence cell growth [32]. We carried out immunoblot analysis to investigate if the effect on growth rate upon reduction of EBV BART miRNA was a result of altered LMP1 expression. SNK6 cells were transfected with either control miRNA (Scramble) or anti-EBV-miR BART9 and cells were lysed 96 hours post-transfection. Immunoblots were performed and probed for LMP1 levels. We found that inhibiting EBV miR-BART9 reduced LMP1 protein expression by almost 50% when normalized to the Hsp70 loading control and relative to the control miRNA (Fig. 4A). In these experiments, we also probed for lytic protein Zta in order to examine if the activation of EBV lytic program was the reason for reduced SNK6 cell growth rate and found no detectable expression of Zta protein (data not shown). We also investigated the kinetics of anti-EBV-miR-BART9 effect on LMP1 level by carrying out a time-course experiment. We observed that there was a ~46% reduction of LMP1 protein level 96 hours post-transfection of anti-EBV-miR-BART9 compared to control miRNA (Fig. 4B).

We next examined if the ~50% reduction in LMP1 protein level following inhibition of BART9 was a consequence of reduced LMP1 mRNA expression. SNK6 cells were transfected with anti-EBV-miR-BART9 and total RNA extracted from the cells 96 hours post-transfection. cDNA was synthesized and Q-PCR was performed using LMP1 specific primers. We found that there was ~2-fold decrease in the LMP1 mRNA levels when BART9 was inhibited (Fig. 4C). This data suggests that BART9 miRNA functions as a positive factor for LMP1 at the level of mRNA accumulation.

EBV miR-BART9 has a positive effect on LMP1 protein and mRNA expression in SNK6 cells

If BART9 does indeed have a positive influence on LMP1 expression, then increasing its level might be predicted to increase LMP1 expression, in contrast to the effect of the antisense BART9 miRNA (Fig. 3, 4). To test this prediction, we transfected a precursor for miRNA-BART9 (pre-EBV-miR-BART9) into SNK6 cells and performed immunoblots and Q-RT-PCR to examine levels of LMP1 protein and mRNA, respectively. We found that increasing BART9 levels increased LMP1 protein expression by ~33% relative to cells transfected with the precursor negative control miRNA (pre-NegCtrl) when normalized to the loading control β-actin (Fig. 5A). We also found that over expressing BART9 increased the LMP1 mRNA level by a factor of 1.7 (Fig. 5B).

A

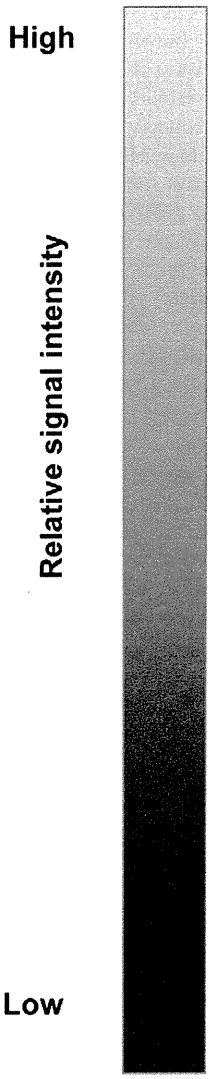

	SNK6	SNT16
ebv-miR-BART17-5p	8,343	10,472
ebv-miR-BART7	7,752	13,936
ebv-miR-BART1-3p	6,283	13,446
ebv-miR-BART9	5,951	12,277
ebv-miR-BART1-5p	5,916	10,270
ebv-miR-BART16	5,447	12,926
ebv-miR-BART14	4,681	7,458
ebv-miR-BART22	4,104	8,655
ebv-miR-BART8*	3,587	7,982
ebv-miR-BART8	3,519	8,180
ebv-miR-BART4	3,352	6,850
ebv-miR-BART19-3p	3,300	3,646
ebv-miR-BART5	2,702	4,046
ebv-miR-BART10	2,056	3,332
ebv-miR-BART12	1,953	2,623
ebv-miR-BART11-3p	1,920	2,347
ebv-miR-BART6-3p	1,834	3,152
ebv-miR-BART18-5p	1,215	4,551
ebv-miR-BART2-5p	1,074	2,122
ebv-miR-BART17-3p	458	904
ebv-miR-BART2-3p	415	1,073
ebv-miR-BART15	56	17
ebv-miR-BART20-5p	46	53
ebv-miR-BART18-3p	44	23
ebv-miR-BART10*	36	0
ebv-miR-BART20-3p	31	25
ebv-miR-BART5*	19	37
ebv-miR-BHRF1-2*	14	37
ebv-miR-BHRF1-2	10	23
ebv-miR-BHRF1-1	9	27
ebv-miR-BHRF1-3	3	16

B

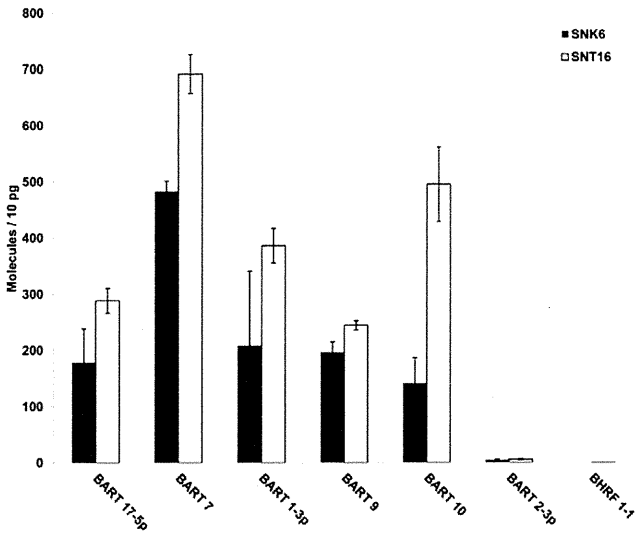

C

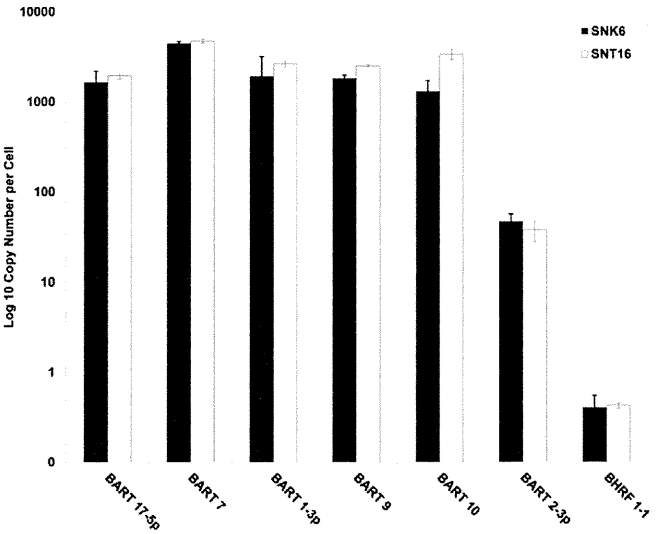

Figure 2. MiRNA expression profile in NK T cell lymphoma cell lines. (**A**) The table shows the median expression values from normalized, log-ratio (base 2) data sets of representative EBV miRNAs in SNK6 and SNT16 cell lines arranged in a descending order of expression levels. (**B**) Taqman qPCR for selected EBV miRNAs in SNK6 and SNT16 cells. The indicated EBV miRNAs were quantified using a stem-loop PCR protocol described by Chen et al [46] for detecting miRNAs. The copy number of each of the miRNAs was determined by reverse transcription and amplification of synthetic miRNAs. The graph represents miRNA expression as molecules per 10 picogram RNA. (**C**) Taqman qPCR for indicated EBV miRNAs in SNK6 and SNT16 cells as described in (B). The data are presented as copy number of EBV miRNA per cell.
doi:10.1371/journal.pone.0027271.g002

Increase in EBV-miRNA-BART9 level modestly affects SNK6 cell growth

The role of LMP1as the oncoprotein of EBV is dependent on its expression level. While LMP1 has been reported to promote cellular transformation, increased expression of LMP1 can inhibit cell growth [33]. We next investigated whether increasing BART9 levels would inhibit SNK6 cell growth. Precursor BART9 was transfected into SNK6 cells and samples were collected every 24 hours for three days and cell numbers and viability analyzed. We found that increasing BART 9 levels modestly (~8%) affected SNK6 cell growth rate (Figure 6A) without affecting viability (Figure 6B). Although the data for reduction in growth rate of SNK6 following over-expression of BART9 did not show a statistically significant difference in a paired t-test, the results of three independent experiments showed a clear and reproducible trend of reduced growth. This suggests that the level of LMP1 needs to be regulated stringently as an increase (Figure 6) or decrease below a threshold point (Figure 3 and 4) has an inhibitory effect on SNK6 cell growth. To determine whether the effects of BART9 miRNA on LMP1 expression are directed through the 3′UTR of the LMP1 mRNA, we cotransfected a BART 9 miRNA precursor with an LMP1 expression plasmid containing the natural 3′UTR and a plasmid lacking this element in HeLa cells. Under these conditions, BART9 had no effect on LMP1 expression from either expression plasmid, suggesting that the effects of BART9 on LMP1 expression are indirect (data not shown).

Discussion

In this study we show that ~20 EBV miRNAs are abundantly expressed in Nasal NK/T cell lymphomas (NKTCL). We also provide evidence that modulating EBV miRNA levels impacts NKTCL growth rate. Furthermore, we found a direct correlation between levels of EBV-miR-BART9 and LMP1 protein and mRNA expression. Together, these observations suggest that BART9 miRNA positively modulates expression of LMP1 and one manifestation of perturbing this regulation is a retardation of NKTCL cell growth.

A number of studies have characterized EBV miRNA expression and their roles in nasopharyngeal carcinomas [4,11,19]. Other studies have focused on the role of cellular miRNAs in NKTCLs [34] and other human cancers [35]. While EBV miRNAs have been found to be conserved evolutionarily [3], they are differentially expressed in different cell types [3,7]. However, to our knowledge this is the first study to determine the expression of EBV miRNAs in NKTCLs. We found that at least 19 EBV miRNAs are abundantly expressed in NKTCLs. Indeed, these 19 miRNAs appear to be expressed at levels 2–3 logs higher than their expression in NPCs [19]. We note that a limitation of our study is that only two NKTCL cell lines and no primary tumors were profiled. Nevertheless, our data suggest that even though EBV viral gene expression might be similar to NPC and Hodgkin disease [36], miRNA expression could vary greatly between these two tumors.

What role might these EBV miRNAs play in NKTCLs? Cancer is a disease where cell proliferation is dysregulated. A number of studies have demonstrated a connection between miRNAs and cellular differentiation and in many instances miRNAs act as oncogenes by down-regulating tumor suppressors [30,37]. In this study, we found that inhibiting EBV miRNAs slowed the growth rate of NKTCLs. This reduction in proliferation was not because of loss of cell viability. These EBV miRNAs may be functionally analogous to cellular miRNAs like miR- 106b that targets the cell cycle inhibitor $p21^{Cip1}$ [38] or miR-221 and miR-222 that regulate $p27^{kip1}$ [39]. Since EBV miRNAs are evolutionarily conserved [3], it is also possible that they target viral proteins as is the case with EBV-miR-BART17-5p that has been reported to regulate LMP1 [11] or EBV-miR-BART2 that down-regulates BALF5 viral DNA polymerase [10]. In the SNK6 cell line we observed that inhibiting EBV-miR-BART9 reduced the level of LMP1 mRNA and protein. Furthermore, over-expression of BART9 miRNA resulted in increase of LMP1 protein and transcript levels. This suggests that in NKTCLs, BART9 miRNA likely regulates LMP1 mRNA expression and we favor the hypothesis that this is an indirect regulation as a reporter plasmid containing the 3′ UTR of the LMP1 mRNA was not responsive to BART9 in transient expression experiments (data not shown). BART9 may indirectly up-regulate LMP1 by targeting a repressor of its expression. When BART9 is inhibited, the level of this putative repressor may be increased resulting in decrease of LMP1 transcript and protein levels. Alternatively, BART9 may be involved somehow in maintaining LMP1 mRNA stability which has been reported to have a long half-life [40]. In this scenario, BART9 may stabilize LMP1 mRNA, and inhibition of BART9 thus renders the LMP1 mRNA susceptible to degradation.

A tight regulation on the expression of LMP1 is beneficial to EBV and its survival in infected cells. For instance, if LMP1 expression is consistently high, it can either result in cell growth arrest [41], inhibit viral and cellular promoters [42] or enhance epitope presentation to cytotoxic T cells [43]. However, under certain conditions, it might be beneficial for EBV to induce LMP1 expression for a short period of time. Notably, a recent study reported the transient upregulation of LMP1 by the p38 signaling pathway [44].

In summary, we have shown that 19 EBV miRNAs are abundantly expressed in NKTCLs and their levels are likely to be important in maintaining cell growth. Our data also indicate that EBV BART9 is involved in regulating LMP-1 expression in these cells. This has implications in mechanisms of lymphomagenesis and future experiments could be directed at investigating the role of EBV miRNAs and its regulation of cellular targets.

Methods

Cell lines

The NK-T cell lymphoma (NKTCL) cell lines, SNK6, SNK10, SNT8, SNT15, SNT16 were obtained from Norio Shimizu (Tokyo Medical and Dental University). The cells were cultured in RPMI1640 supplemented with 10% fetal bovine serum, 1%

A

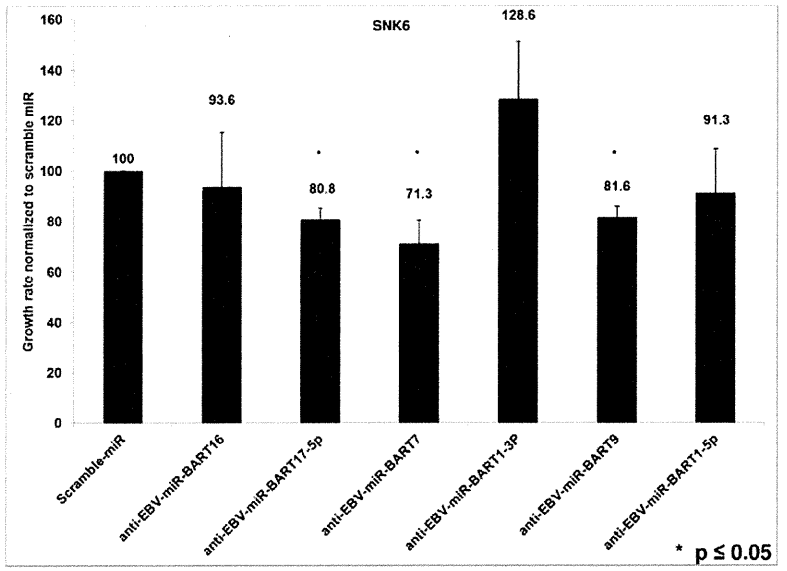
SNK6
Growth rate normalized to scramble miR
160
140
120
100
80
60
40
20
0
100
93.6
80.8
71.3
128.6
81.6
91.3
Scramble-miR
anti-EBV-miR-BART16
anti-EBV-miR-BART17-5p
anti-EBV-miR-BART7
anti-EBV-miR-BART1-3P
anti-EBV-miR-BART9
anti-EBV-miR-BART1-5p
* p ≤ 0.05

B

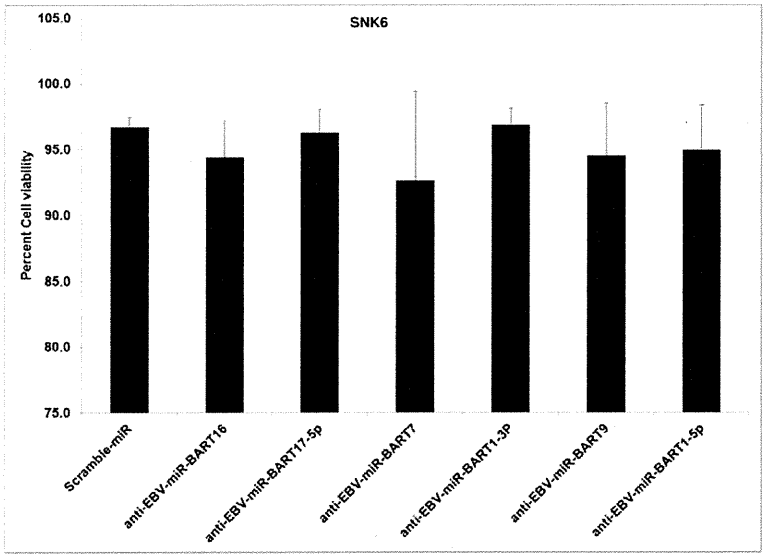
SNK6
Percent Cell viability
105.0
100.0
95.0
90.0
85.0
80.0
75.0
Scramble-miR
anti-EBV-miR-BART16
anti-EBV-miR-BART17-5p
anti-EBV-miR-BART7
anti-EBV-miR-BART1-3P
anti-EBV-miR-BART9
anti-EBV-miR-BART1-5p

C

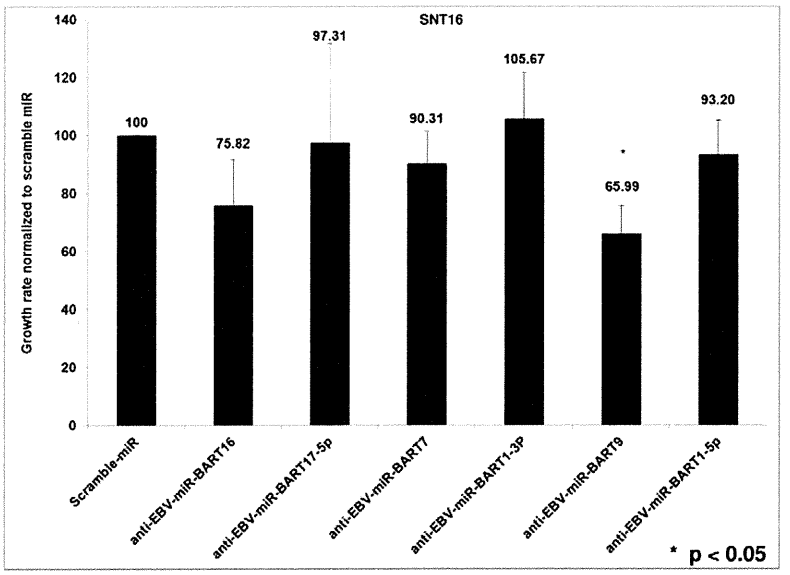
SNT16
Growth rate normalized to scramble miR
140
120
100
80
60
40
20
0
100
75.82
97.31
90.31
105.67
65.99
93.20
Scramble-miR
anti-EBV-miR-BART16
anti-EBV-miR-BART17-5p
anti-EBV-miR-BART7
anti-EBV-miR-BART1-3P
anti-EBV-miR-BART9
anti-EBV-miR-BART1-5p
* p < 0.05

Figure 3. Inhibiting EBV BART miRNA levels affect NKTCL growth rate without affecting cell viability. (**A**) SNK6 cells were transfected with antisense to the indicated EBV miRNAs and cell numbers counted every 24 hours for three days. Cell growth rate was calculated as difference in cell numbers between the 24 hour and 72 hour time point and compared with cells transfected with control Scramble miRNA. Data shown are the average ± SD from three independent experiments. (* represents p value of ≤0.05 in a paired t-test). (**B**) SNK6 transfected with antisense EBV miRNAs were analyzed for viability by Trypan blue exclusion in a Vi-CELL counter every 24 hours for three days. The data presented is the cell viability at 72 hours post-transfection and is the average ± SD from three independent experiments. (**C**) SNT16 cells were transfected with antisense to the indicated EBV miRNAs and cell growth rate analyzed as described above. Data shown are the average ± SD from three independent experiments. (* represents p value of <0.05 in a paired t-test).
doi:10.1371/journal.pone.0027271.g003

Penicillin-Streptomycin and 250 ng/ml Fungizone (Amphotericin B; Invitrogen) and 600 IU of IL-2.

MiRNA microarray analysis and validation

Total RNA was isolated from SNK6 and SNT16 cells using the miRNAeasy kit (Qiagen) as per manufacturer's protocol. RNA was analyzed by LC Sciences (Houston, TX) with miRNA microarrays using the μParaflo microfluidic chip technology and all data is MIAME compliant. The detailed process can be found at http://www.lcsciences.com. Briefly, photogenerated reagent chemistry probes for miRNAs were *in situ* synthesized on chips with three repeats for each probe to allow for statistical analysis. MiRHumanViruses version 13 arrays were used to detect a total of 1100 unique mature miRNAs comprising of 875 human miRNAs and 225 virus miRNAs. The virus miRNAs included 44 EBV miRNAs. RNA samples from SNK6 and SNT16 cells were labeled with Cy3 for hybridization. The chips included 50 control probes based on Sanger miRBase Release 13 with four-sixteen repeats. The control probes were used for quality controls of chip production, sample labeling and assay conditions. Included in the control probes were PUC2PM-20B and PUC2MM-20B which are the perfect match and single-base match detection probes, respectively, of a 20-mer RNA positive control sequence that is spiked into the RNA samples before labeling. For a transcript to be listed as detectable three conditions had to be met: (1) signal intensity had to be greater than three times background standard deviation; (2) spot co-variance (CV), defined as ratio of standard deviation over signal intensity had to be less than 0.5; (3) the signals from at least 50% of the repeating probes had to be above detection level. Data was normalized using a cyclic LOWESS (Locally-weighted Regression) method [45] to remove system related variations such as sample amount variations, dye labeling bias, and signal gain differences between scanners to reveal biological relevant variations. A t-test was performed on the signals obtained for the repeating probes and p-value calculated. MiRNAs were defined as differentially expressed if they had a p-value<0.01. Clustering analysis was performed with a hierarchical method using average linkage and Euclidean distance metric. The clustering data was represented as a heat map using TIGR MeV (Multiple Experimental Viewer; The Institute for Genomic Research). The microarray data has been deposited in GEO database with accession number GSE30695.

Validation of miRNA microarray

Selected EBV miRNAs were quantified using a PCR protocol described by Chen *et al* [46] for detecting miRNAs. Briefly, stem-loop primers complementary to specific EBV miRNAs were designed as described by Cosmopoulos *et al* [19]. For each miRNA assayed, 100 ng of total RNA was reverse transcribed using a TaqMan MicroRNA RT kit as described by the manufacturer and a specific stem-loop primer at a final concentration of 50 nM. RNA was prepared using an RNeasy kit (Qiagen) from exponentially growing tissues culture cells. Each 20 ul PCR reaction contained 1 ul of RT product, 1×TaqMan Universal master mix, 1.5 uM forward primer, 0.7 uM reverse primer, and 0.2 uM probe. The reactions were incubated in a 48-well plate at 95°C for 3 min, followed by 40 cycles of 95°C for 15 s and 60°C for 30 s. The copy number of each of the miRNAs was determined by reverse transcription and amplification of synthetic miRNAs that were identical to the published sequences.

miRNAs and transfection

The miRCURY locked nucleic acid (LNA) modified antisense oligonucleotides to EBV BART miRNAs (anti-EBV-miR-BART) were purchased from Exiqon. The sequence of the antisense oligonucleotides are as follows: Scramble Negative Control (5′-GTGTAACACGTCTATACGCCCA -3′); anti-EBV-miR-BART9 (5′- ACTACGGGACCCATGAAGTGTTA- 3′); anti-EBV-miR-BART17-5p (5′- CTTGTATGCCTGCGTCCTCTTA-3′); anti-EBV-miR-BART7 (5′- CCCTGGACACTGGACTATGATG-3′); anti-EBV-miR-BART1-3p (5′- GACATAGTGGATAGCGGTG-CTA-3′); anti-EBV-miR-BART1-5p (5′- CACAGCACGTCAC-TTCCACTAAGA-3′); anti-EBV-miR-BART16 (5′FAM- AGAG-CACACACCCACTCTATCTAA-3′). Precursor EBV miRNA (pre-EBV-miR) was designed based on the sequence in miRBase sequence database (http://microrna.sanger.ac.uk/sequences). pre-EBV-miR-BART9 (5′- UAACACUUCAUGGGUCCCGUAGU-3′) and precursor Negative control miRNA (pre-NegCtrl) were ordered from Ambion/Applied Biosystems.

SNK6 and SNT 16 cells were seeded at 1×10^6 cells in 24- well tissue culture plates and transfected with antisense or precursor miRNAs using Oligofectamine or Lipofectamine RNAimax according to the manufacturer's protocol. Transfection efficiency of the miRNAs in SNK6 and SNT 16 cells was determined with FAM labeled EBV- BART16 miRNA and was found to be nearly 98% as determined by flow cytometry (data not shown). Cell viability following transfections was measured by Trypan Blue exclusion and found to be ~95%.

RT-real time PCR for EBV mRNAs

Independent transfections of anti-EBV-miR-BART 9 or pre-EBV-miR-BART 9 were performed in SNK6 cells. The controls transfected were either Scramble-miRNA (Exiqon) or Precursor-Negative Control (Pre-NegCtrl) (Applied Biosystems), respectively, as described above. Total RNA was isolated using RNeasy mini kit (Qiagen) and RT-real-time-PCR assays carried out for quantification of LMP1 and α-tubulin levels using the Bio-Rad MyIQ single color detection system. Briefly, 10 ng of cellular RNA was reverse transcribed into cDNA using the iScript cDNA synthesis kit (Bio-Rad) in a 20 μl reaction using the manufacturer's protocol. Quantitative real-time PCR was performed using 3 μl of the synthesized cDNA and the iQ™ SYBR Green Supermix (Bio-Rad). PCR reactions were carried out in 96-well format using a Bio-Rad iCycler. Analysis was done by the MyIQ software program (Bio-Rad) and the fold-changes were calculated using the ΔΔCt method as previously described [47] with α-Tubulin as the housekeeping gene control. The primer sequences used for LMP1 have been described previously [48] and were LMP1 (forward) - 5′

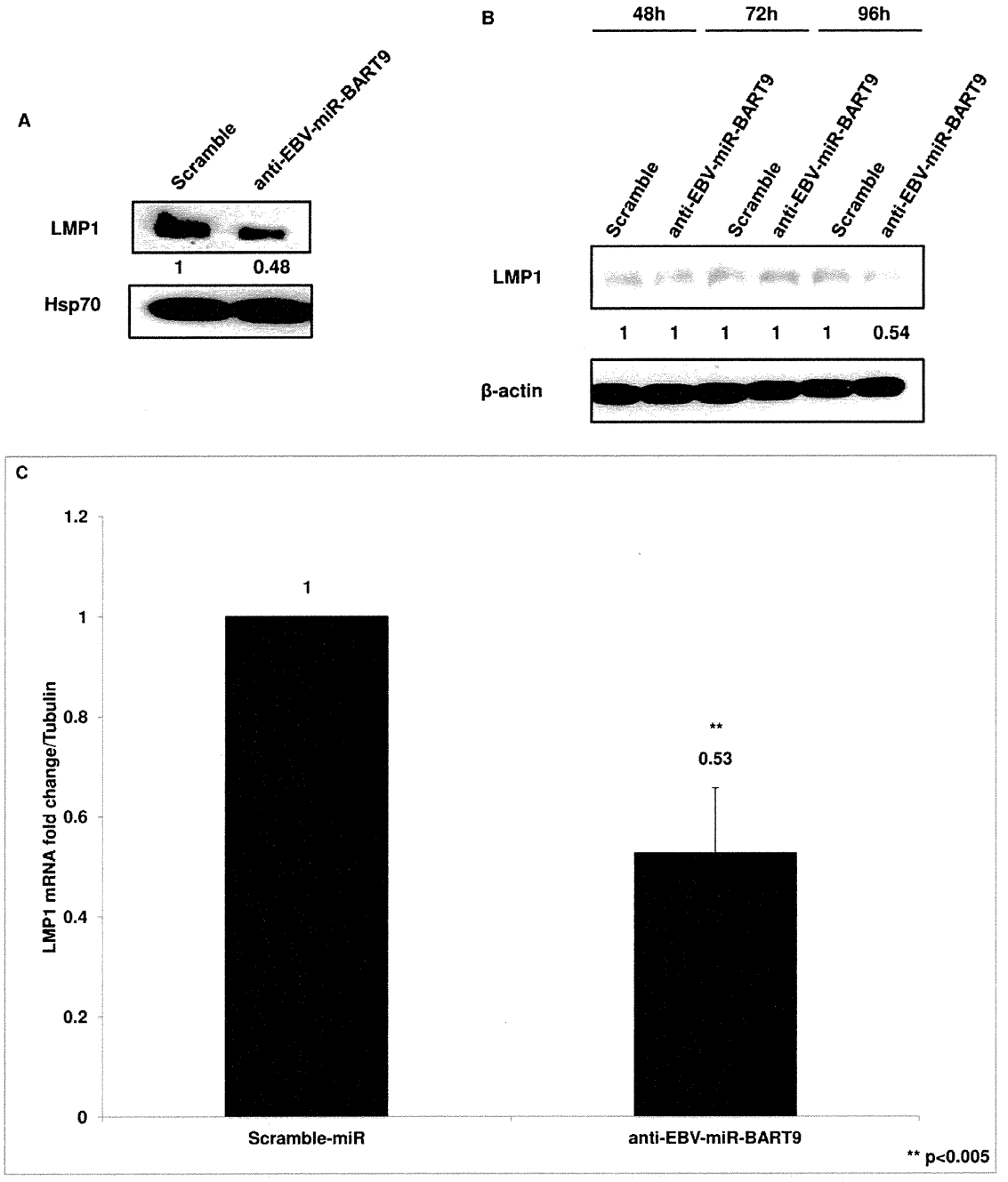

Figure 4. Immunoblot and Q-RT-PCR analysis of LMP1 expression in SNK6 following inhibition of EBV-BART9 miRNA. (**A**) SNK6 cells were transfected with anti-EBV-BART9 miRNA or Scramble control miRNA and cell lysates prepared 96 hours post-transfection. LMP1 protein expression was analyzed in immunoblots. When compared to cells transfected with control miRNA and normalized to β-actin loading control, quantification of immunoblots showed that BART9 inhibition reduced LMP1 protein levels by ~50%. (**B**) SNK6 cells were transfected with control or anti-EBV-BART9 miRNA and samples collected every 24 hours in a time-course experiment. Cell lysates were prepared and immunoblot analysis carried out to determine LMP1 expression. Quantification of LMP1 levels using Image J as described above showed that LMP1 protein levels are reduced only at later time-point. (**C**) SNK6 cells were transfected with either anti-EBV-BART9 or control miRNA and cells collected 96 hours post-transfection. Total RNA was extracted and cDNA synthesized using iScript cDNA synthesis kit. Using LMP1 specific primers, Q-PCR was carried out and data analyzed using the ΔΔCt method. Data shown is the average ± SD from three independent experiments. (** represents p value of <0.005 in a paired t-test).
doi:10.1371/journal.pone.0027271.g004

AGCCCTCCTTGTCCTCTATTCCTT 3′, LMP1 (reverse) - 5′ACCAAGTCGCCAGAGAATCTCCAA 3′. The primers for α-Tubulin were, α-Tubulin (forward) - 5′ CCTGACCACCCACACCACAC 3′, α-Tubulin (reverse) - 5′ TCTGACTGATGAGGCGGTTGAG 3′.

Cell proliferation functional assay

SNK6 and SNT16 cells were seeded in 96 well plates at 8×10^5 cells in 100 µl/well and transfected with 100 pmol of indicated anti-EBV-miRNAs or pre-EBV-miRNAs or control Scramble-miRNA or Pre-Neg-Ctrl. In some experiments, the cells were

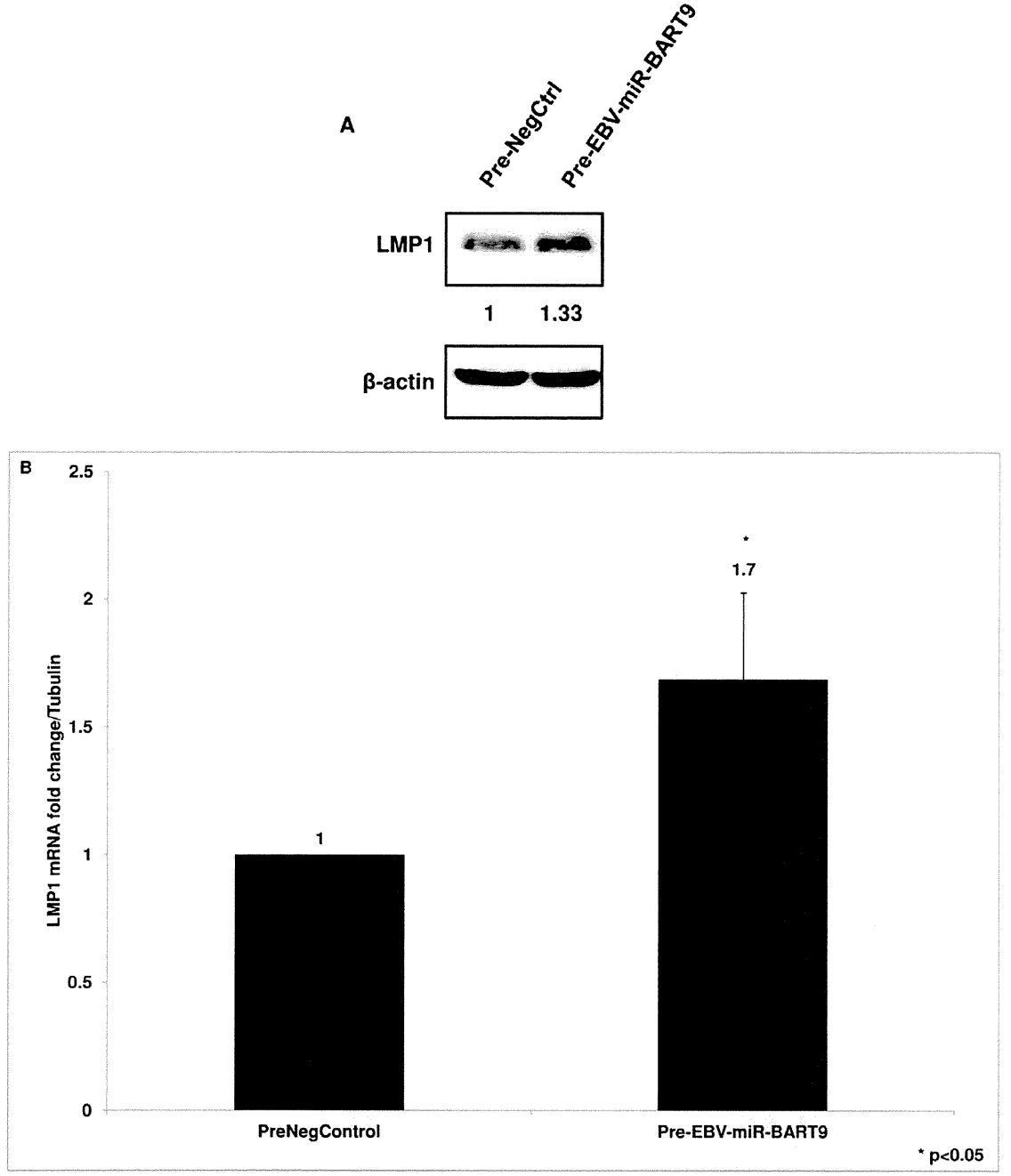

Figure 5. Precursor EBV-BART9 miRNA increases LMP1 protein and mRNA levels in SNK6 cells. (**A**) SNK6 cells were transfected with precursor EBV-BART9 or control miRNA. The cells were collected 96 hours post-transfection and cell lysates prepared for immunoblot analysis. Quantification of immunoblots showed a ~33% increase in LMP1 protein levels in cells transfected with EBV miRNA compared to control miRNA transfected cells when normalized to loading control. Data shown is a representative immunoblot from three independent experiments. (**B**) Total RNA was extracted from SNK6 cells transfected with precursor EBV-BART9 or control miRNA. Following cDNA synthesis, LMP1 mRNA levels were analyzed by Q-RT-PCR. Data presented is the average ± SD from three independent experiments. (* represents p value of <0.05 in a paired t-test).
doi:10.1371/journal.pone.0027271.g005

seeded at 1×10^6 cells/well. After overnight incubation, the cells were transferred into 24 well tissue culture plates. Cells were collected every 24 hours and analyzed for cell number and viability using the Becton-Dickinson Vi-CELL counter at the Baylor College of Medicine Flow Cytometry Core. The cell counter uses trypan blue exclusion to automatically stain and count cells, as well as assay cell size and viability.

Immunoblotting

Cells following treatment were lysed with EBCD buffer (50 mM Tris-HCl, pH 8.0, 120 mM NaCl, 0.5% NP-40, 5 mM dithiothreitol) containing protease inhibitor cocktail (Sigma). Immunoblotting was performed as described previously [49]. Monoclonal antibodies used in this study include, LMP1 (S12), EBNA-LP (JF186), EBNA3C (A10), and EBNA2 (R3). Other antibodies

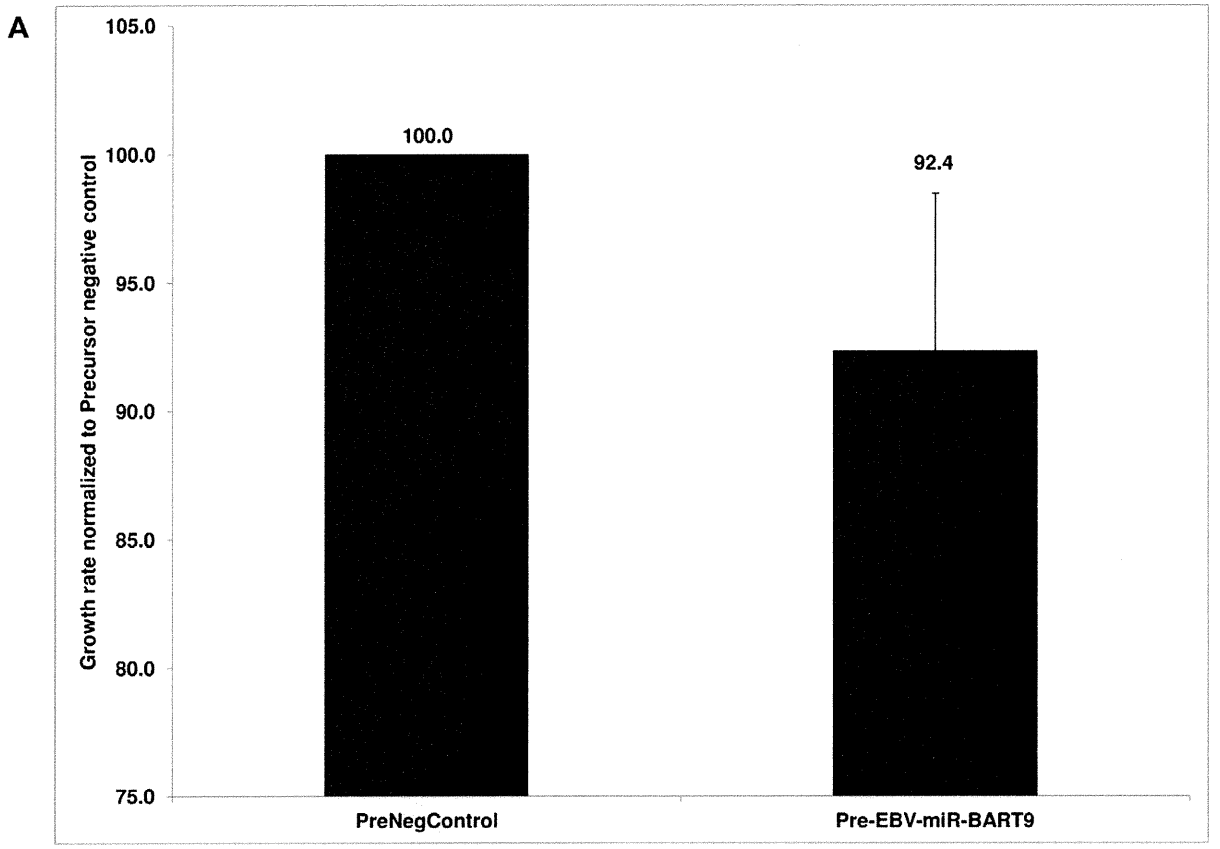
A
105.0
100.0
95.0
90.0
85.0
80.0
75.0
Growth rate normalized to Precursor negative control
100.0
92.4
PreNegControl
Pre-EBV-miR-BART9

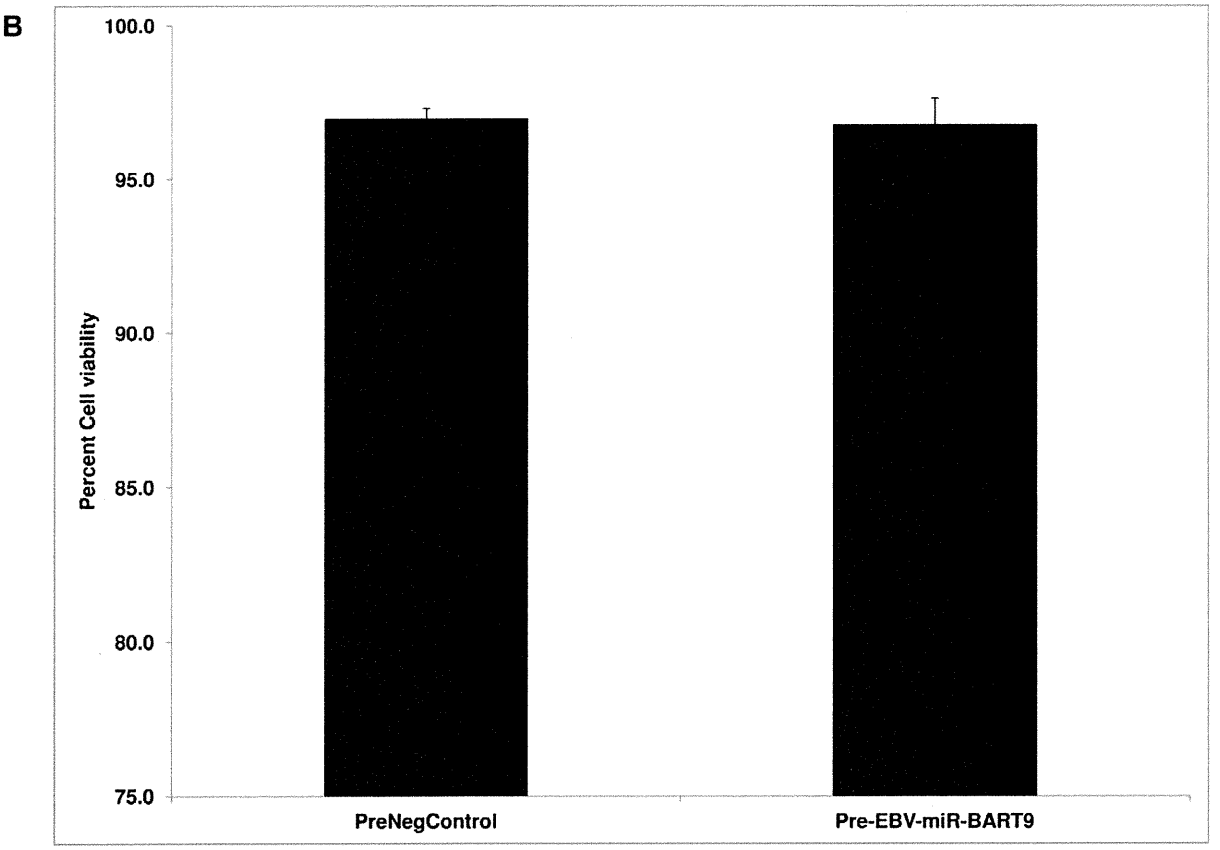
B
100.0
95.0
90.0
85.0
80.0
75.0
Percent Cell viability
PreNegControl
Pre-EBV-miR-BART9